Trnp1 Regulates Expansion and Folding of the Mammalian Cerebral Cortex by Control of Radial Glial Fate

Ronny Stahl, 1,2,3 Tessa Walcher, 3 Camino De Juan Romero, 5 Gregor Alexander Pilz, 3 Silvia Cappello, 3 Martin Irmler, 4 José Miguel Sanz-Aquela,⁶ Johannes Beckers,^{4,7} Robert Blum,^{1,9} Víctor Borrell,⁵ and Magdalena Götz^{1,2,3,8,*}

¹Physiological Genomics, Institute of Physiology, Ludwig-Maximilian University Munich, Schillerstrasse 46, 80336 Munich, Germany

Helmholtz Center Munich, Ingolstädter Landstrasse 1, 85764 Neuherberg, Germany

⁵Instituto de Neurociencias, Consejo Superior de Investigaciones Cientificas-Universidad Miguel Hernandez, 03550 Sant Joan d'Alacant, Spain

⁶Service of Pathology, Hospital Universitario "Principe de Asturias," 28805 Alcalá de Henares, Spain

http://dx.doi.org/10.1016/j.cell.2013.03.027

SUMMARY

Evolution of the mammalian brain encompassed a remarkable increase in size of the cerebral cortex, which includes tangential and radial expansion. However, the mechanisms underlying these key features are still largely unknown. Here, we identified the DNA-associated protein Trnp1 as a regulator of cerebral cortex expansion in both of these dimensions. Gain- and loss-of-function experiments in the mouse cerebral cortex in vivo demonstrate that high Trnp1 levels promote neural stem cell self-renewal and tangential expansion. In contrast, lower levels promote radial expansion, with a potent increase of the number of intermediate progenitors and basal radial glial cells leading to folding of the otherwise smooth murine cerebral cortex. Remarkably, TRNP1 expression levels exhibit regional differences in the cerebral cortex of human fetuses, anticipating radial or tangential expansion. Thus, the dynamic regulation of Trnp1 is critical to control tangential and radial expansion of the cerebral cortex in mammals.

INTRODUCTION

During mammalian evolution, brain regions were dynamically adapted by selective growth and expansion with a high degree of specificity. An impressive example is the expansion of the mammalian neocortex resulting in profound gyrification to accommodate an enormous increase in neuronal cell numbers (Lui et al., 2011). Notably, distinct brain regions can be expanded selectively in specific species, such as for example the auditory cortex in bats (Krubitzer, 2007; Martínez-Cerdeño et al., 2012). However, the mechanisms regulating evolutionary changes in size of specific brain regions still remain poorly understood.

Regulation of specific stem and progenitor cells during development is closely linked to control of the size of brain regions (Krubitzer, 2007; Fish et al., 2008; Borrell and Reillo, 2012). In particular, expansion of regions within the cerebral cortex occurs in two dimensions: tangential and radial growth (Rakic, 1995). Tangential growth is mediated by expanding neural stem cell (NSC) populations, such as neuroepithelial and radial glial cells (RGs), anchored at the apical surface in the ventricular zone (VZ) (Götz and Huttner, 2005). To increase the number of neurons per area, radial growth is achieved by either a prolonged phase of neurogenesis or through addition of germinal layers beyond the VZ (Rakic, 1995), such as the subventricular zone (SVZ) that is further expanded to an inner and outer SVZ (iSVZ and oSVZ, respectively) in the cerebral cortex of mammals with a larger neocortex, including primates (Smart et al., 2002; Lui et al., 2011; Borrell and Reillo, 2012). In the murine cerebral cortex, the SVZ largely comprises basal progenitors (BPs), which increase the number of neurons generated per time and area (Götz and Huttner, 2005). Besides increased numbers of BPs, additional RGs that have lost their apical anchor and are only connected to the basement membrane (BM) are incorporated in the SVZ (Smart et al., 2002; Fietz and Huttner, 2011; Lui et al., 2011; Reillo et al., 2011; Borrell and Reillo, 2012). Intriguingly, high numbers of such basal radial glia (bRG) correlate with a high gyrification index of the cerebral cortex (Fietz et al., 2010; Hansen et al., 2010; Lui et al., 2011; Reillo et al., 2011; Reillo and Borrell, 2012). In contrast, only few bRG are present in the SVZ of lissencephalic cerebral cortices with a smooth surface (Reillo et al., 2011; Shitamukai et al., 2011; Wang et al., 2011). Notably, the ventricular surface of gyrated brains is smooth, whereas the basal surface is folded due to an increase in gray



²Munich Center for Integrated Protein Science CIPSM, Butenandtstrasse 5-13, 81377 Munich, Germany

³Institute of Stem Cell Research, German Research Center for Environmental Health

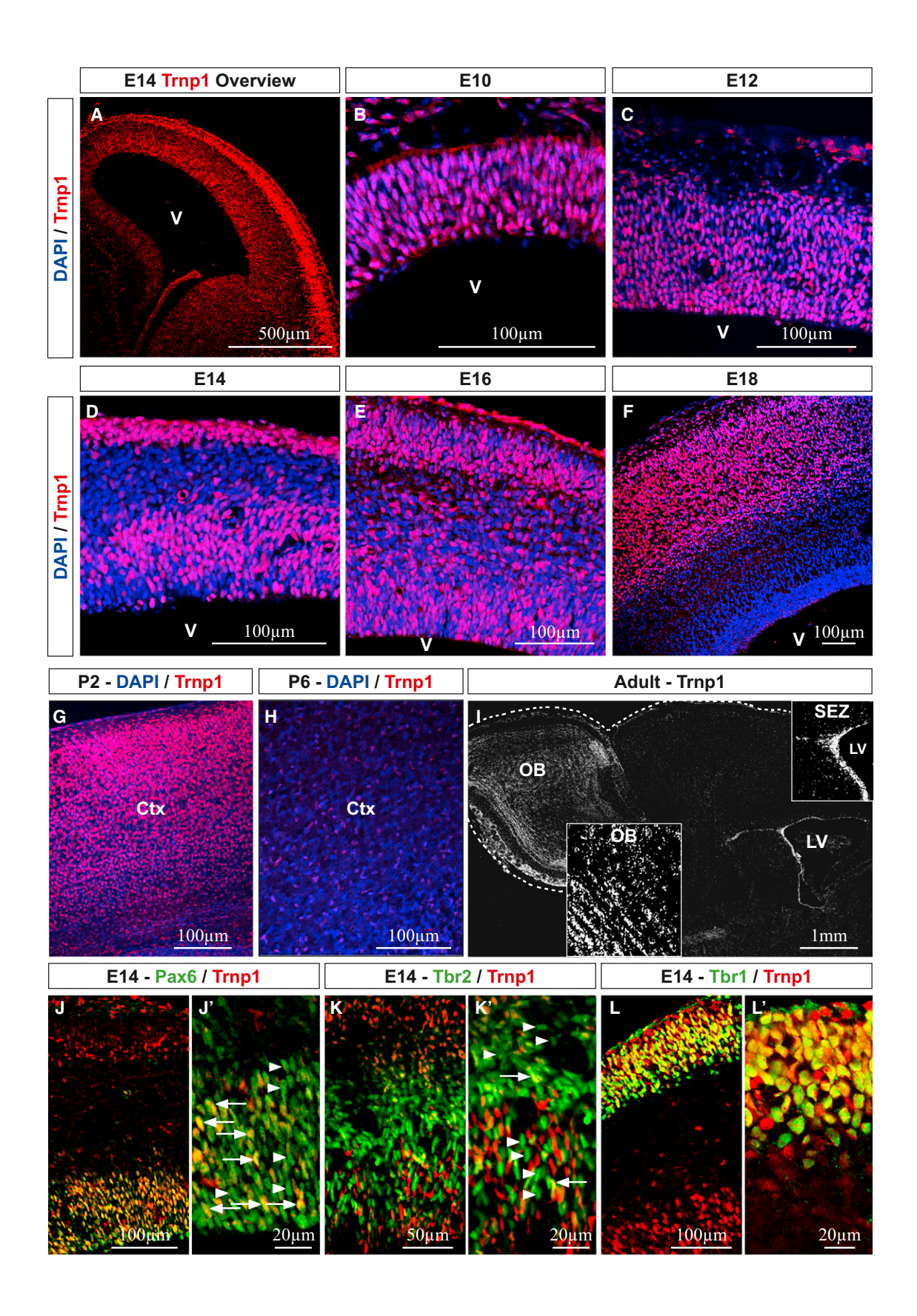
⁴Institute of Experimental Genetics

⁷Technical University Munich, Chair of Experimental Genetics, 85350 Freising-Weihenstephan, Germany

⁸Munich Cluster for Systems Neurology (SyNergy), 80336 Munich, Germany

⁹Present address: Institute for Clinical Neurobiology, University of Würzburg, 97078 Würzburg, Germany

^{*}Correspondence: magdalena.goetz@helmholtz-muenchen.de



and white matter comprising neurons and glia (Borrell and Reillo, 2012). Therefore, gyrification reflects coordination of radial expansion and lateral dispersion of neurons in the cortical plate (CP), which is in profound contrast to a mere overproliferation resulting in an overall folded epithelium (Chenn and Walsh, 2002). This highlights how tangential, radial, and lateral expansion modes must be coordinated during cerebral cortex development and gyrification. Thus, a fascinating question in brain development and evolution is how such complex processes are regulated at the molecular and cellular level.

We set out to search for regulators of radial glia (RG) fate in an unbiased manner by genome-wide expression analysis of RG subpopulations that differ in the generation of BPs (Pinto et al., 2008). The screen was confirmed by the transcription factor AP2γ (identified at higher levels in RG generating BPs) that promotes the generation of BPs (Pinto et al., 2009). In order to identify regulators promoting the maintenance of RG rather than the generation of BPs, we selected a gene with higher expression in the subset of RG generating few BPs for further analysis: Trnp1 (formerly known as 2300002D11Rik; Pinto et al., 2008). TMFregulated nuclear protein Trnp1 has so far only been described as a nuclear protein in immortalized cell lines (Volpe et al., 2006); however, its in vivo function remained unknown. Intriguingly, Trnp1 sequence is very different in nonmammalian vertebrates, whereas it shows clear sequence conservation among mammals (86% in human-mouse orthologs). Because its protein sequence does not carry any known motif or domain (Volpe et al., 2006) and Trnp1 has, to our knowledge never been studied during development or in any in vivo context, we examined first its expression and then its function in the developing cerebral cortex.

RESULTS

Trnp1 Is Specifically Expressed in a Subset of RG and in **Newborn Neurons during Cerebral Cortex Development**

We generated a specific antibody against Trnp1 (Figures S1A-S1D available online) and examined its localization in the developing forebrain from embryonic day 10 to 18 (E10-E18). Trnp1 was exclusively localized to the nucleus in apical progenitors (APs) in the VZ and newborn neurons in the CP (Figure 1A). Interestingly, Trnp1 immunoreactivity decreased significantly during development with virtually all cells in the VZ being Trnp1+ at E10 to no detectable immunoreactivity at E18, the end of neurogenesis (Figures 1B-1F). We noted some degree of cellular heterogeneity in Trnp1 immunoreactivity that remained higher in a subset of Pax6+ RG in the VZ, whereas virtually no Tbr2+ BPs in the SVZ expressed Trnp1 (Figures 1J-1K'). This is consistent with our previous results identifying lower levels of Trnp1-mRNA expression in RG generating BPs (Pinto et al., 2008). Thus, Trnp1 is expressed in an everdecreasing subset of Pax6+ cells in the VZ, suggestive of an expression in self-renewing NSCs whose number declines during development.

Notably, also the expression of Trnp1 in neurons (as confirmed by double staining with the neuronal marker Tbr1) was transient and vanished within the first postnatal week (Figures 1G, 1H, 1L, and 1L'). At later postnatal stages and in the adult brain, virtually no Trnp1 immunoreactivity was detectable except for one region of adult neurogenesis: the subependymal zone (SEZ) of the lateral ventricle from where newborn neurons migrate via the rostral migratory stream (RMS) to the olfactory bulb (OB; Figures 1I and S1E-S1G). However, cells in the other neurogenic niche, the dentate gyrus, did not express Trnp1 (Figure S1H). Taken together, Trnp1 protein expression is highly restricted to the phase of neurogenesis and Trnp1 remains expressed in the adult neurogenic region with the highest amplification and neuronal output.

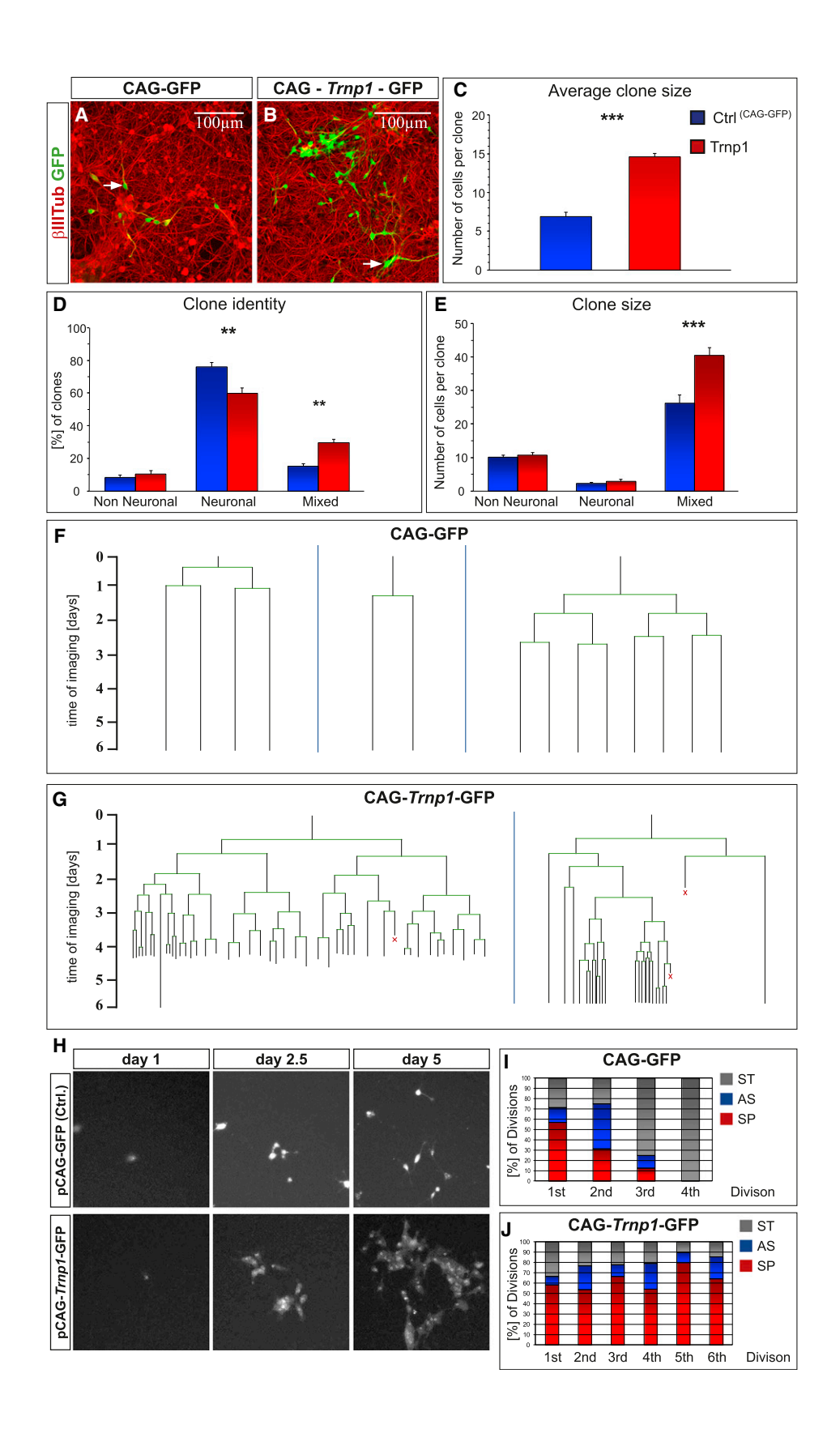
Trnp1 Increases Proliferation of Neural Stem Cells

Because the aforementioned expression pattern suggested a potential role of Trnp1 in neural stem or progenitor cells, we aimed at determining its function by gain- and loss-of-function approaches. Toward this aim, we cloned Trnp1 cDNA into a bicistronic retroviral vector with the chicken β-actin (CAG) promoter driving the expression of Trnp1 and GFP linked by an internal ribosomal entry site (IRES) (see Heinrich et al., 2011; Figure S2A). After confirmation of reliable coexpression of GFP and Trnp1 by immunostaining (Figures S2B and S2C), we utilized this virus to overexpress Trnp1 in progenitor cells from dissociated cultures of the E14 cerebral cortex. By use of less than 25 viral particles per well, we ensured clear separation of clones representing the progeny of initially a single infected cell (note that retroviral vectors only integrate into dividing cells; Haubst et al., 2004; Costa et al., 2008). Interestingly, clones transduced with Trnp1 virus contained more than double the number of cells as compared to clones infected with the control virus 7 days posttransduction (Figures 2A-2C), suggesting a profound increase in proliferation.

To determine the composition of these enlarged clones, we stained for the neuron-specific protein ßIII-tubulin, and progenitor and glia markers Nestin and GFAP (Figures 2A, 2B, S2D, and S2E). This allowed distinguishing (1) NSC clones (clones with "mixed" identity comprising \$\text{BIII-tubulin+ neurons and \$\text{BIII-}} tubulin- glia or progenitor cells); (2) neuronal clones (all cells βIII-tubulin+); and (3) nonneuronal clones (comprising glial and progenitor cells, but no βIII-tubulin+ cells) (Figures 2A, 2B, and 2D). Trnp1 overexpression significantly increased the percentage of mixed, stem cell clones at the expense of pure neuronal clones (Figure 2D). Interestingly, the proportion of nonneuronal clones was not increased, suggesting that high levels of Trnp1

Figure 1. Endogenous Trnp1 Expression in the Developing and Adult Brain

(A-I) Images of coronal (A-H) or sagittal (I) sections of the developing (A-H, E10-P6) and adult (I; composite of single confocal images created by a Zeiss Tile scan) cerebral cortex (Ctx) labeled for Trnp1 and DAPI. Note that Trnp1 expression is restricted to neurogenic regions. LV, lateral ventricle; V, ventricle. (J-L') Trnp1 is expressed in a subpopulation of Pax6+ RG (J and J') and Tbr1+ neurons (L and L'), whereas it is largely absent in Tbr2+ BPs (K and K') in E14 cerebral cortex. Arrows indicate examples of double-positive cells; arrowheads point to Pax6+ or Tbr2+ cells that do not express Trnp1. See also Figure S1.



do not suppress the generation of neurons per se but, rather, increase self-renewal of NSCs still allowing neurogenesis to occur. Consistent with this, clone size selectively increased in mixed clones, whereas purely neuronal or purely nonneuronal clones were not affected by Trnp1 overexpression (Figure 2E). In order to gain further insights into the mechanism by which the mixed clones increase in size, we used continuous live-cell imaging as described before by Costa et al. (2008) and Asami et al. (2011). Although most cells infected with the control virus generated largely postmitotic daughter cells after two or three rounds of division (Figures 2F, 2H, and 2I), Trnp1-transduced cells still gave rise to proliferating progeny after six rounds of cell division (Figures 2G, 2H, and 2J). Thus, clone size increased due to an increased rate of cell-cycle reentry and symmetric proliferative divisions, whereas the average cell-cycle length was not affected (18.9 hr in control and 18.4 hr upon Trnp1 overexpression). Taken together, these results suggest a role of Trnp1 in cell fate regulation, with high levels of the protein promoting NSC fate maintaining their proliferative potential and inhibiting symmetric terminal divisions that give rise to neuron-only clones (see Costa et al., 2008; Asami et al., 2011).

Trnp1 Increases Proliferation of APs and Inhibits the **Generation of BPs In Vivo**

Our in vitro data raised the question to what extent forced Trnp1 expression may also promote proliferation of NSCs in vivo. To analyze this question, we electroporated pCAG-Trnp1-IRES-GFP or the control vector pCAG-IRES-GFP into E13 cerebral cortices and examined the brains 3 days later at E16. Upon Trnp1 overexpression, we observed a consistent overall increase in the number of GFP immunoreactive cells and a tangential expansion of the electroporated area (compare Figures 3B and 3B' to 3A and 3A') with many cells still residing in progenitor areas (Figures 3A-3D'). Quantification confirmed that the majority of Trnp1-electroporated cells (56%) still resided in the VZ and SVZ (Figures 3D, 3D', and 3G) even 3 days after electroporation, whereas most control-electroporated cells had left the VZ (Figure 3C, bottom). Because many cells in the VZ were weakly GFP+ upon Trnp1 overexpression (suggestive of a high proliferation rate and dilution of the electroporated plasmid and protein; Figure 3D, bottom), we examined the proportion of cells in S phase based on their incorporation of the pyrimidine analog bromodeoxyuridine (BrdU) 1 hr before sacrifice. Remarkably, Trnp1 overexpression led to a significant 3× increase in proliferating (BrdU+) cells compared to the control (Figures 3E, 3F, 3H, and S2F). Consistent with the endogenous expression of Trnp1 in a subset of Pax6+ cells, Trnp1 overexpression significantly increased the proportion of Pax6+ APs at the expense of BPs and neurons in the intermediate zone (IZ) and CP (Figures 3E', 3F', 3G, 3I, and 3J). Thus, Trnp1 promotes tangential expansion (Figures 3A–3B') by increasing Pax6+ apical NSCs and reducing the generation of Tbr2+ BPs in vivo. This finding is consistent with the endogenously higher expression levels of Trnp1 in RG that do not generate BPs (Pinto et al., 2008) and with our in vitro findings of Trnp1 promoting self-renewal of NSCs (Figures 2D and 2E).

Knockdown of Trnp1 Increases the Number of BPs and Leads to Radial Expansion of the Developing Cerebral Cortex In Vivo

To determine if Trnp1 is also necessary for RG self-renewal in vivo, we cloned three different small hairpin RNAs (shRNAs) targeting the 3' UTR of Trnp1 mRNA into pSUPER.GFP (expressing both the shRNA and GFP; Figure S3A). Western blotting and immunostaining identified shRNA #1 and shRNA #5 as most effective in reducing Trnp1 protein levels (Figures S3B and S3C), which were then used for in utero electroporations. In pronounced contrast to overexpression, knockdown of Trnp1 at E13 resulted in a significant increase in the proportion of cells located in the CP 3 days after electroporation (Figures 4A-4B' and 4F). Interestingly, in 13 of 14 electroporated embryos (Table S1), we observed a clear radial expansion of the developing cerebral cortex in the electroporated region as compared to the nonelectroporated hemisphere and to controls (compare Figure 4A' with 4B'; see Figures S3D-S3F' for additional examples). As predicted, the number of Pax6+ APs was reduced 3 days after electroporation of either shRNA (Figures 4H and S4D), whereas the proportion of Tbr2+ BPs was significantly increased with both shRNA #1 and shRNA #5 (Figures 4C–4E, 4I, and S4E). This also explains why the overall number of proliferating cells is unchanged (Figure 4G). Notably, the increased number of BPs correlated with a thicker SVZ (compare Figure 4A' with 4B'; and see Figures S3D-S3F'). To our surprise, Tbr2 immunoreactivity revealed a wide scattering of some Tbr2+ cells toward very basal regions (Figure 4E) reminiscent of the expanded, diffuse Tbr2+ band described in the oSVZ of ferrets, macaques, and humans (Reillo and Borrell, 2012; Martínez-Cerdeño et al., 2012; Bayatti et al., 2008).

As further control for the specificity of the observed effects, we aimed at rescuing the increased generation of Tbr2+ BPs upon RNAi by coexpressing an shRNA-resistant form of Trnp1 (lacking the targeted 3' UTR of Trnp1, which we tested for shRNA resistance before; see Figure S3B'). Electroporation of shRNA against endogenous Trnp1 with simultaneous expression of

Figure 2. Effects of Trnp1 Overexpression In Vitro

(A and B) Representative images of GFP+ cells in dissociated cultures from the cerebral cortex isolated at E14 infected with a low titer of either CAG-IRES-GFP control (A) or CAG-Trnp1-IRES-GFP virus (B) immunostained for GFP and \$\textit{\begin{align*} III-tubulin 7 days postinfection. Arrows indicate examples of double-positive cells.} \) (C-E) Histograms depicting quantitative changes in size (C and E) and identity (D and E) of the progeny of single infected cells (clones) after Trnp1 transduction revealing increased number and size of mixed clones containing βIII-tubulin+ and βIII-tubulin- cells. Data are shown as mean ± SEM from four independent experiments. Statistical analysis was performed with the Student's t test in (C) and ANOVA with Tukey's posthoc test in (D) and (E): **p < 0.01 and ***p < 0.001. Blue bars indicate control (Ctrl) virus: red bars show Trnp1 virus.

(F-J) Time-lapse analysis of cells described above showing representative lineage trees obtained by single-cell tracking (F and G; X indicates cell death), representative fluorescence micrographs of GFP+ cells in live imaging (H), and the histograms depicting the frequency of symmetric terminal (ST), asymmetric (AS), and symmetric proliferative (SP) divisions at each round of division (I and J; 14 clones each from two independent experiments). See also Figure S2.

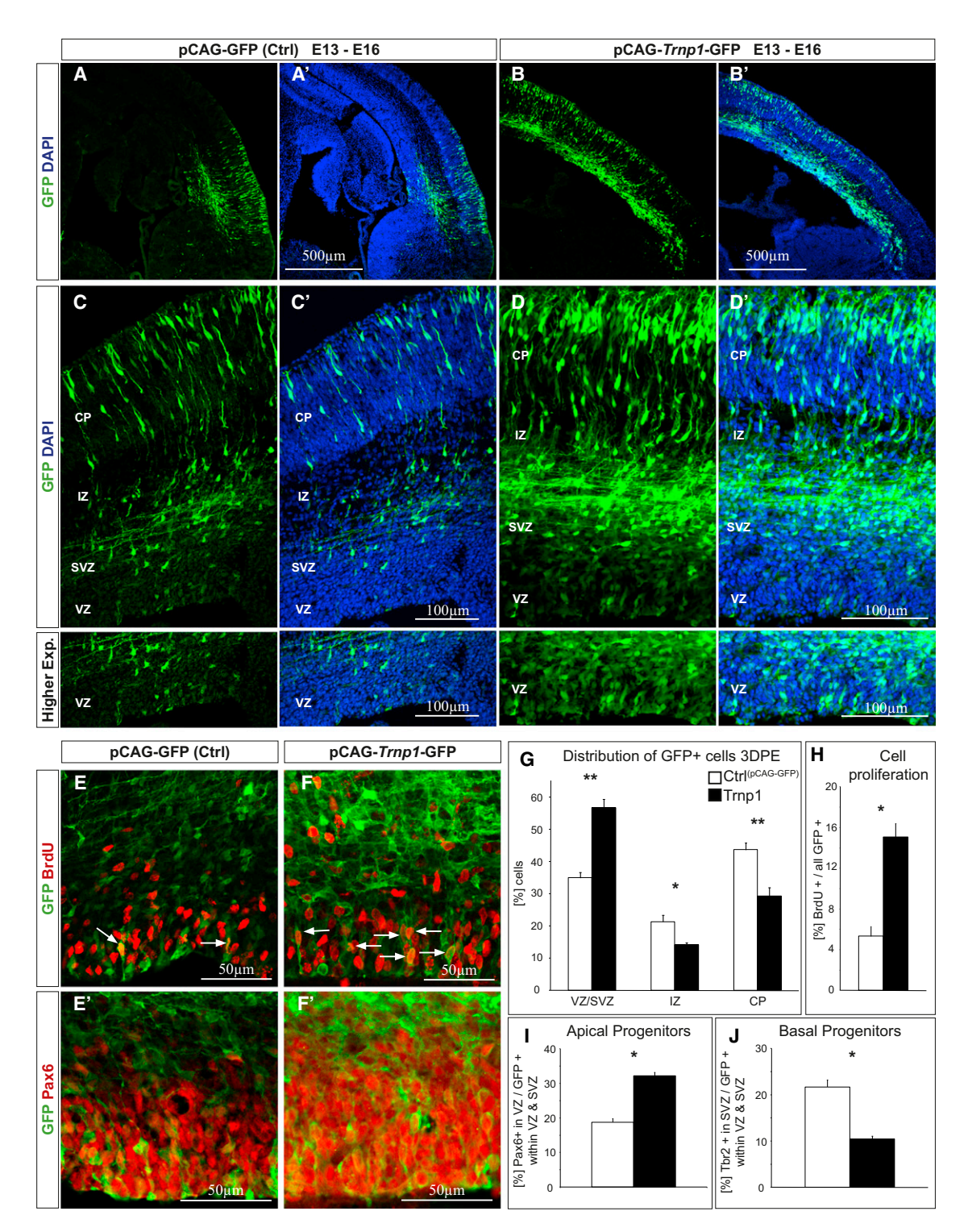


Figure 3. Overexpression of Trnp1 In Vivo Increases AP Numbers and Tangential Expansion

(A-F) Micrographs depicting sections of the cerebral cortex 3 days after electroporation at E13 with either pCAG-IRES-GFP control or pCAG-Tmp1-IRES-GFP plasmid with overviews in (A)-(B'), zooms of the electroporated area in (C)-(D'), with higher exposure of the VZ in the bottom panels of (C)-(D'), and double labeling for BrdU (E) and (F) and Pax6 in (E') and (F').

(G-J) Note the tangential expansion of the electroporated area (A-B') due to increased numbers of APs (C-F') as revealed by quantifications shown in the histograms upon Trnp1 overexpression.

Data are shown as mean \pm SEM from five embryos for cellular localization analysis (G), three for cell proliferation, and four for AP and BP analysis (H \rightarrow J): *p < 0.05 and **p < 0.01, Mann-Whitney U test. See also Figure S2.

shRNA-resistant Trnp1 was able to rescue the increase of Tbr2+ BPs to a level comparable to the control situation (Figures 4I-4J'). Importantly, radial expansion of the cortex was also prevented in five out of five rescue-electroporated embryos, thereby clearly demonstrating the specificity of the effects observed upon Trnp1 knockdown. These results strongly support the previously described role of BPs in radial expansion of the neocortex (Haubensak et al., 2004; Farkas et al., 2008; Fietz and Huttner, 2011; Borrell and Reillo, 2012) and identify Trnp1 as a nuclear regulator of this process.

Trnp1 Knockdown Leads to Increased Production of bRG and Subsequent Gyrification of the Cerebral Cortex

Given the radial expansion and increased number of Tbr2+ cells after Trnp1 knockdown, we asked to what extent also bRG may be increased under these conditions, bRG are characterized by their expression of Pax6, the location of their nucleus in the outer (basal) area of the SVZ, together with the lack of an apical process (Fietz et al., 2010; Hansen et al., 2010; Reillo et al., 2011; Shitamukai et al., 2011; Wang et al., 2011). Remarkably, after Trnp1 knockdown, many Pax6+ cells were found to be located in basal SVZ areas beyond the dense band of Tbr2+ cells (Figures 5A-5B). These cells were clearly separated from the VZ where the vast majority of Pax6+ cells are normally located in the murine brain. Consistent with a bRG identity, these cells possessed a long basal but no apical process (Figures 5C and 5C') and were clearly different from VZ RG and also from SVZ BPs, which are multipolar. These cells are RG and undergo proliferation as indicated by the phosphorylation of vimentin in M phase (Figure 5D). Quantification and comparison with the nonelectroporated (control) hemisphere of the same brain section further confirmed the significant (more than three times) increase of basal Pax6+ cells located beyond the dense Tbr2+ band (Figure 5E). Their bRG identity was further corroborated because most (two out of three) were Tbr2-/Pax6+ upon Trnp1 knockdown, whereas in control, only a minority of the few Pax6+ cells at these basal positions are Tbr2- (Figure 5F). To follow these bRG by live imaging, we sliced cerebral cortices electroporated with shRNA against Trnp1 together with constructs to clonally label the cytoplasm with EGFP and the membrane with mKO2-F (Shitamukai et al., 2011). Brains were sliced 24 hr after electroporation, and live imaging was performed to visualize the processes of dividing cells as previously described by Shitamukai et al. (2011). Interestingly, already 24 hr after electroporation of shRNA targeting Trnp1, many labeled cells had delaminated and lost their apical but still retained a basal process. When following these cells more closely, we could clearly observe bRG undergoing cell division in the typical mode with the basal daughter cell inheriting the basal process (Figure 5G).

Because the increased number of bRG provides additional guides for radially migrating neurons, this typically results in a fanning out of such processes in gyrated cerebral cortices (Lui et al., 2011; Reillo et al., 2011; Borrell and Reillo, 2012). Indeed, RC2 immunostaining revealed the general trajectory of RG processes in the Trnp1shRNA-electroporated cerebral cortex demonstrating that radial fibers fanned out when entering the CP (Figures 5H and 5H'). Most strikingly, we even observed folding of the neocortex within the electroporated area in about 63% of the cortices electroporated with shRNA against Trnp1 at E13 (Figures 5I-5L'; Table S1; n = 24). These folds were notably different from neuronal ectopias such as observed in cobblestone lissencephaly (also known as lissencephaly type II) because the BM was fully intact in case of Trnp1 knockdown (Figures S4F-S4F"), and both sulci and gyri could be followed from rostral to caudal levels (see Figures 5I-5I"). Figures 5I-5I" show a brain 3 days postelectroporation with small sulci at more rostral levels (Figure 5I) developing into a more extended fold at further caudal regions (Figures 5I' and 5I"). Most importantly, analysis of long-term survival of shRNA-electroporated brains showed increasing gyrification with several macroscopic folds apparent at postnatal stages (Figures 5K-5L'), demonstrating that these are not transient structures but further enlarge during development. Remarkably, we observed a higher frequency of folding in cerebral cortices left to develop into postnatal stages after electroporation with Trnp1 knockdown (Table S1). This suggests that the brains without visible folds at E16 either did not yet have sufficient time to develop bigger folds, or they were missed and interpreted as "only" expansion due to sectioning limitations such as the angle of cutting. However, even without considering such cases, the overall efficiency of emerging folds upon knockdown of Trnp1 still comprised twothirds of all brains (Table S1), representing an amazing frequency given the normally lissencephalic nature of the murine cerebral cortex.

Given the high frequency of such folds developing in the cerebral cortex upon Trnp1 knockdown, we set out to observe this also by live imaging. The brains were sliced 24 hr after electroporation with shRNA (plus pCAG-GFP for better visualization of the cells) or pCAG-GFP alone as a control, and low-magnification imaging was performed 48 hr later. Following the overall development of the tissue and cells upon Trnp1 knockdown (Movie S1) allowed visualization of a strikingly fast and robust radial and lateral movement of many GFP-labeled cells that followed the paths of additional bRG fibers (compare Movies S1 and S2; see postimaging 3D reconstruction in Movie S3 and Nestin staining in Figures S4G-S4G"; both showing the slice shown in Movie S1). Additionally, these movies confirmed the increase in delamination from the apical surface and increased proliferation at more basal positions (Movie S4) and also revealed a rather fast migration of newborn neurons upon Trnp1 knockdown (Movie S1 compared to Movie S2). Thus, live imaging revealed several coordinated cell biological events contributing to an apparent gyrification in the murine cerebral cortex.

Because delamination of cells occurred almost too fast to visualize this by live imaging, we returned to still analysis in sections and examined the cleavage plane of APs, as increased oblique or horizontal cell divisions had been previously shown to result in increased bRG production (Shitamukai et al., 2011). Consistent with this, 24 hr after shRNA electroporation, we observed a clear shift toward horizontally oriented cleavage angles, thus generating daughter cells lacking an apical contact prone to delaminate from the ventricular surface (Figures S5A) and S5B). Taken together, downregulation of Trnp1 leads to cortical expansion and folding in a dual mode. First, reduced Trnp1 levels lead to delamination and increased generation of both BPs and bRGs. This results second in increased production

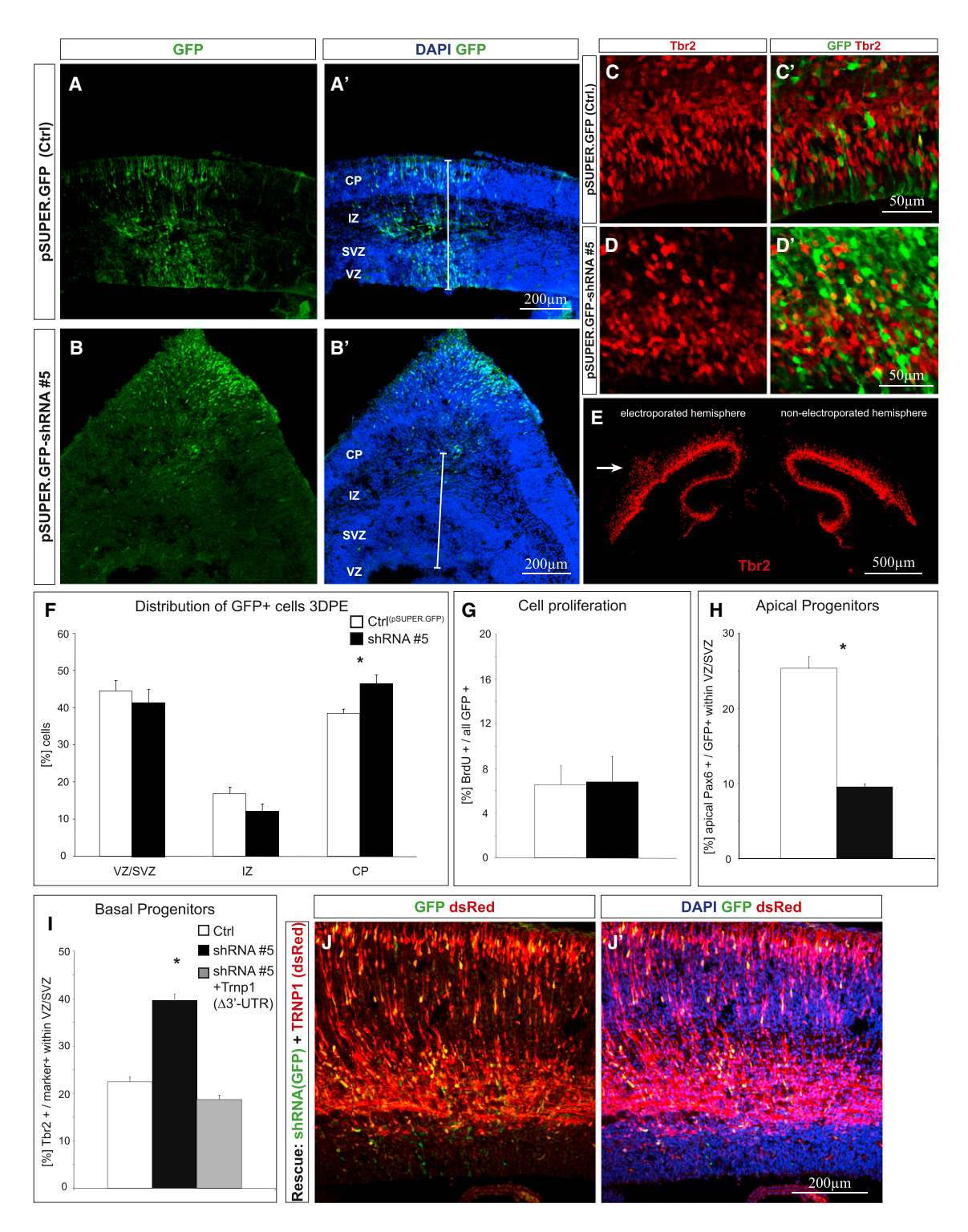


Figure 4. Knockdown of Trnp1 In Vivo Increases the Number of BPs

(A-E) Micrographs of sections of the cerebral cortex analyzed at E16 3 days postelectroporation (DPE) with either pSUPER.GFP control or pSUPER.GFPshRNA plasmid to knock down Trnp1. Note the strong radial expansion of shRNA-electroporated cortices as visible by the white bar in (A') and (B') indicating the radial length of the control-electroporated cortex and the increase of Tbr2+ cells (C-D'), which spread further basally (white arrow in E; reconstruction of one coronal section of an shRNA-electroporated cerebral cortex), absent on the control side (right in E) or after control vector electroporation.

(F-I) Histograms depict the quantification of GFP+ cells (F), their proliferation (G), and progenitor identity (H and I) in these experiments (black bars indicate shRNA; white bars show control).

(legend continued on next page)

of neuron numbers as well as increased bRG fibers that serve as guiding structures. Altogether, such processes cause a lateral dispersion of higher neuron numbers within the CP and ultimately lead to folding of the otherwise lissencephalic murine cerebral cortex.

Trnp1 Is Tightly Associated with DNA and Is Involved in **Transcriptional Activation**

Given the exciting cell biological functions of Trnp1, we examined its localization within the nucleus more closely to gain insights into its molecular function. Endogenous Trnp1 is homogeneously distributed in euchromatin regions but not detectable in heterochromatin (Figures S5C and S5D). However, in contrast to most transcription factors that dissociate from chromatin in M phase, Trnp1 remained tightly associated with condensed chromosomes during mitosis in vivo and in vitro (Figures S5E, S5F, and S5I-S5I").

In standard SDS-PAGE analysis, recombinant Trnp1 appears in different bands with a relative molecular weight ranging from 23 to 30 kDa (Figure S1C). This pattern is also observed when endogenous Trnp1 is isolated from brain tissue (Figures S5G and S5H). To test the stringency of Trnp1-DNA interaction, we used an acidic lysis protocol generally used to release basic proteins such as histones from DNA. Strikingly, acidic lysis was not stringent enough to release Trnp1 protein from the nuclear fraction of the developing cerebral cortex at E14. Despite successful release of histones, Trnp1 still remained in the insoluble fraction (Figure S5G). Interestingly, a GFP-fusion construct of Trnp1 no longer showed the strong DNA association of Trnp1 (Figures S5J-S5J"), possibly due to structural alterations of the protein. This fusion protein was also no longer functional because electroporation of the Trnp1-GFP fusion construct was not able to reproduce the overexpression phenotype (Figures S5K and S5L). We thus conclude that the tight DNA association is essential for the molecular function of Trnp1.

Given the role of Trnp1-DNA interaction, we next examined to what extent changes of Trnp1 levels directly affect the transcriptome. We collected RNA from GFP+ cells (isolated by fluorescence-activated cell sorting [FACS]; see Figures S6A-S6B"') 22-24 hr after electroporation at E13. A gene expression analysis on Affymetrix Gene ST 1.0 arrays revealed a total of 152 differentially expressed probe sets (44 upregulated, 108 downregulated) upon Trnp1 downregulation as compared to control-electorporated samples (p < 0.01, fold changes of >1.5, and average expression >50 in at least one group; Figure 6B). Notably, Trnp1 mRNA was significantly downregulated with a linear ratio of knockdown versus control of 0.76 (p < 0.01) (Figure 6A), and random samples of the differentially expressed genes were confirmed by qPCR (Figure S6C). Trnp1 knockdown predominantly resulted in reduced gene expression levels. Gene Ontology term analysis showed a significant (p < 0.01) enrichment of terms related to transcriptional regulation (e.g., DNA binding, transcriptional repression or activation, RNA metabolic processes, regulation of gene expression). Specifically, downregulation of Trnp1 resulted in an early response of (1) bHLH transcription factors that play a role in neural differentiation such as NeuroD1/NeuroD2/NeuroD6 and Rnd2; (2) chromatin-remodeling factors such as Chd7, Bmi1, Nuak1, and Smarca5; and (3) histone variants (Hist3h2a, Hist4h4, Hist1h4f, Hist1h4c), which (except for Chd7) were all downregulated. Importantly, no celltype-specific genes were altered, showing that the time point of analysis (22-24 hr after shRNA electroporation) was sufficiently early to exclude secondary effects based on altered cellular compositions (e.g., apical [Pax6+] or basal [Tbr2+] progenitors). Thus, the observed changes reflect early alterations in gene expression upon Trnp1 knockdown revealing the role of this nuclear protein in activating transcription either directly or indirectly in tight association to euchromatin.

TRNP1 Is Expressed in the Human Developing Brain with **Local Differences Correlating with Gyrification**

Given the profound effect of Trnp1 on gene expression and the aforementioned phenotype with high levels provoking tangential and low levels resulting in radial expansion, we asked whether Trnp1 may also be expressed in the same layers in the developing human cerebral cortex. In situ hybridization of cerebral cortex sections obtained from specimen at gestational weeks (gws) 12, 18, and 21 (times of early to very late cortical neurogenesis, respectively; Rakic, 1995) revealed a highly specific signal of TRNP1 mRNA in the developing human brain (no signal was detectable using sense riboprobes; data not shown). Reminiscent of its expression pattern in the murine cerebral cortex, we observed high expression levels in the VZ and in neurons in the CP with rather low expression in the SVZ, where BPs and bRGs are located (Figures 6C-6G). Interestingly, we noted regional differences of TRNP1 expression in the VZ, which were more pronounced at gws 18 and 21 (see Figures 6D and 6E for an overview). Lower levels of TRNP1 were found in germinal layers of cortical areas that are known to undergo greater expansion and folding later during development, such as the occipital (Figures 6D and 6D') and temporal lobes (Figures 6E, 6E', and 6F), whereas higher levels of TRNP1 were observed in cortical regions that will undergo little radial expansion and folding, such as the precentral (Figures 6D and 6D") and parahippocampal gyri (Figures 6E, 6E", and 6G). These data suggest that TRNP1 plays a central role in mammalian brain development, and differential regulation of its expression levels may be crucial to define the patterns of cortical folding observed in gyrated brains.

DISCUSSION

In this study, we identified Trnp1 as a regulator of mammalian brain development and as a key factor controlling neocortical expansion. Trnp1 levels have striking effects on tangential, radial, and lateral expansion of the cerebral cortex (summarized

(J and J') Micrographs of the rescue experiments with coelectroporation of the shRNA against Tmp1 together with the shRNA-resistant form of Tmp1 and the quantification of resulting BPs in (I) (gray bar shows rescue of the increase in BPs elicited by Trnp1 knockdown). Data are shown as mean ± SEM from five embryos for cellular localization (F), four for APs and BPs (H and I), and three for cell proliferation analysis (G): *p < 0.05, Mann-Whitney U test. See also Figure S3 and Table S1.

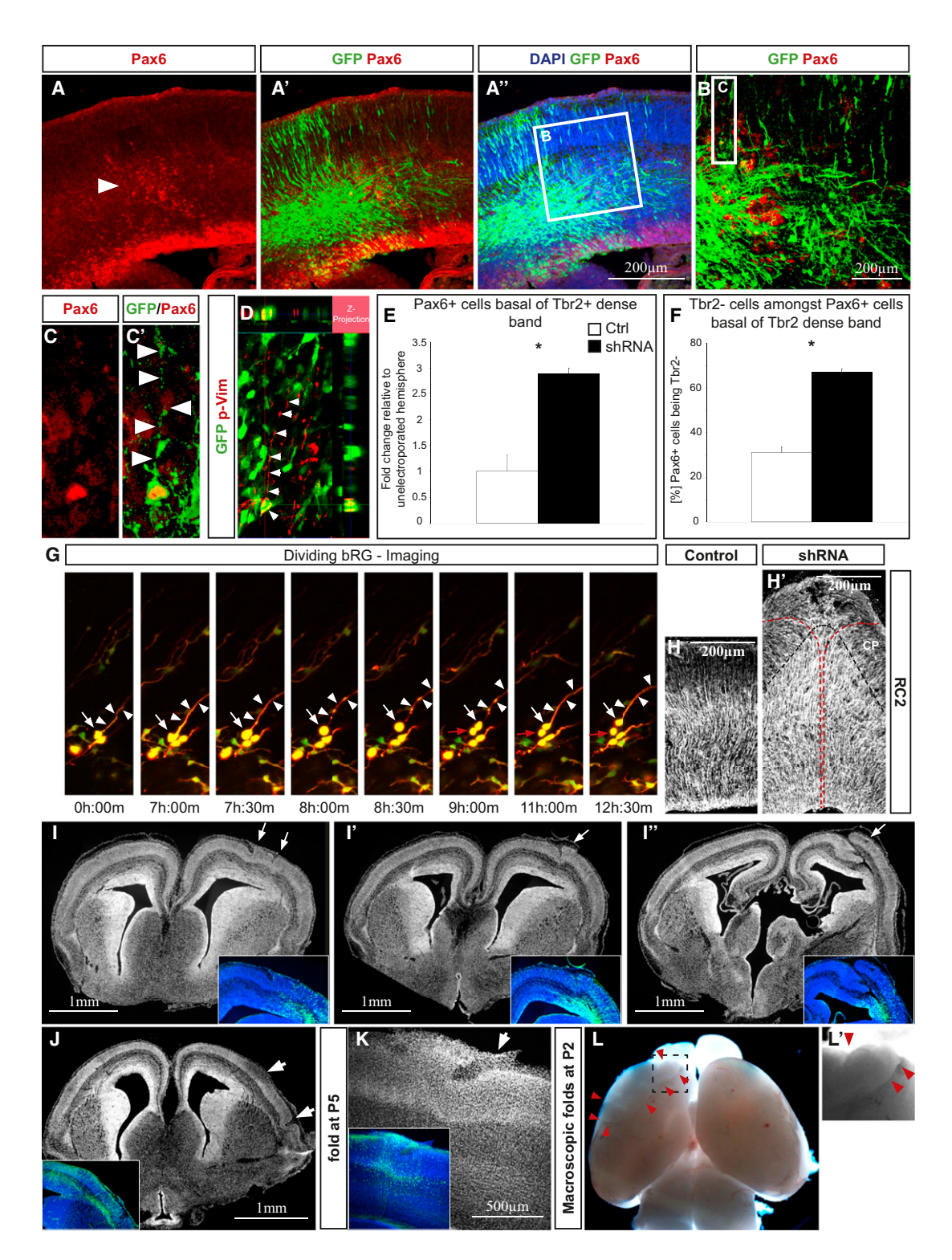


Figure 5. Knockdown of Trnp1 Increases the Number of bRGs and Induces Folding

(A–D) Micrographs of coronal sections from E16 cerebral cortex electroporated at E13 with shRNA against Trnp1 showing more Pax6+ bRG (arrowhead in A) residing far outside the normally Pax6+ VZ (bottom in A–A") and higher magnifications (B–C') of the areas indicated in (A") and (B), respectively. A Z-maximum projection identifying the basal process is shown in (C) and (C'). (D) bRG observed upon knockdown of Trnp1 are p-Vim positive.

(E and F) Histograms of the number of Pax6+ cells at the site of electroporation residing basal of the Tbr2+ dense band (E) (more than 200 μ m away from the ventricle) and (F) the percentage of Tbr2- cells among Pax6+ cells counted in (E). Note the significantly increased number of Pax6+ cells in regions basal to the SVZ after Trnp1 knockdown. Data are shown as mean \pm SEM from three embryos: *p < 0.05, Mann-Whitney U test.

(legend continued on next page)

in a model in Figure 7). Raising the levels of Trnp1 by overexpression promotes self-renewing RG cell fate, thereby increasing the pool of apically anchored stem cells and causing a tangential expansion of the electroporated region within the murine cerebral cortex (Figures 7A and 7A'). Conversely, lowering the levels of Trnp1 increases the generation of both BPs and bRGs, thereby causing a considerable radial expansion including the formation of gyrus/sulcus-like structures with lateral dispersion of neurons in the CP (Figures 7B and 7B'). Thus, Trnp1 is shown to regulate the generation of apical RG (aRG) versus bRG and BPs at the same time. Therefore, Trnp1 qualifies as a master regulator of RG fate. Furthermore, its manipulation provides a mouse model for gyrification, allowing studying such processes also at the cellular and molecular level.

Mechanisms of Trnp1 Function

Overexpression and knockdown experiments suggest that the levels of Trnp1 expression are crucial for the regulation of tangential versus radial expansion and the choice between apical or basal RG. Importantly, endogenous levels of Trnp1 differ between different subsets of RG: RG generating (Tbr2+) BPs express lower levels of Trnp1, which was the basis for its previous identification by Pinto et al. (2008). Conversely, self-renewing apical RG have higher Trnp1 levels, and their decreasing number during development is reflected by reduced numbers of Trnp1+ cells in the VZ. A role for high levels of Trnp1 in promoting self-renewal of RG was further evident by overexpression in vitro with self-renewing NSCs expanding by cell-cycle reentry and symmetric proliferative divisions and in vivo with increasing Pax6+ and BrdU-incorporating cells in the VZ. Trnp1 overexpression also enhanced proliferation in a breast cancer cell line by promoting G1/S transition (Volpe et al., 2006), suggesting that Trnp1 may act at various levels in regulating proliferation. Indeed, we showed here that it also affects the orientation of cell divisions in the developing cerebral cortex.

However, Trnp1 is also expressed in postmitotic voung neurons, and despite its relevance in regulating proliferation, it is important to note that Trnp1 is not generally expressed in all proliferative cells. It is absent in highly proliferative cell lines such as HEK, NRK, or ES cell-derived neural progenitors (data not shown), in BPs and in glial progenitors in vivo and in vitro (data not shown). Thus, Trnp1 is a key regulator of cell fate controlling specific aspects in stem or progenitor cells rather than serving as a common regulator of proliferation.

Trnp1 appears to require extraordinarily strong DNA interaction for its intriguing functions. Although endogenous Trnp1 remained associated with condensed chromosomes during mitosis (contrary to most transcription factors), a Trnp1-GFP

fusion protein dissociated from the chromatids during mitosis. The fusion construct could not promote the increase in Pax6+ NSCs but rather exhibited a partial loss-of-function phenotype in vivo, suggesting that this fusion protein may also interfere with the function of the endogenous protein. This effect may be mediated by the formation of helix bundles with the endogenous Trnp1. The central part of the protein contains either one long or multiple short helices (whereas the Nand C-terminal ends are rather unstructured as revealed by in silico analysis) and a strikingly high number of arginines (10%) resulting in its highly basic nature (PI around 12). A similarly high proportion of arginines is found in the protein sequence of UTF1 (van den Boom et al., 2007), which has the capacity to affect chromatin compaction (Kooistra et al., 2010). Intriguingly, genome-wide expression analysis after knockdown of Trnp1 revealed that many of the differentially regulated genes are involved in chromatin regulation, for example chromatin remodeling factors such as Smarca5, Bmi1, Chd7, ccdc101, and several histone variants (Table S2). In addition, mRNA levels of some transcription factors of the NeuroD or zinc finger families were altered (Table S2). Importantly, none of the classical hallmarks for cell or progenitor types was altered in expression in this analysis, demonstrating that we do not monitor the outcome of cell fate changes but rather the very first targets of Trnp1 regulated by its tight association with DNA and chromatin.

Gyrification in the Mouse Cerebral Cortex

Beyond its molecular functions, manipulating Trnp1 levels in vivo resulted in dramatic alterations in mouse cerebral cortex development, culminating in gyrus formation in the brain of this naturally lissencephalic animal. The development of gyrification involves generating a very large number of neurons per ventricular surface area (i.e., per apical RG; radial expansion) and providing these cells with the adequate scaffold to translate their radial migratory movement into lateral dispersion in the CP. In gyrated mammals, this radial expansion and lateral dispersion of neurons is achieved by a dramatic increase in neurogenic progenitor cells and the massive formation of bRG in the oSVZ, which are critical to lead radially migrating neurons into lateral dispersion (Dehay and Kennedy, 2007; Borrell and Reillo, 2012). Remarkably, knockdown of Trnp1 alone was sufficient to induce a rapid progression from apical RG into both BPs and bRG in vivo in the mouse cerebral cortex. In contrast to the normally rather inefficient generation of bRG in the murine cerebral cortex (Shitamukai et al., 2011; Wang et al., 2011), the generation of unusually large numbers of BPs and bRGs after Trnp1 knockdown leads to the formation of a thickened SVZ resembling the

⁽G) Sequences of a time-lapse movie following a dividing bRG in a cerebral cortex slice prepared at E14 24 hr after electroporation with Trnp1 shRNA and plasmids for Cre, FloxP-EGFP, and mKO2-F for sparse cytoplasmic and membrane labeling (Shitamukai et al., 2011). White arrows and arrowheads indicate the bRG before and after cell division; red arrow indicates the multipolar daughter cell lacking a basal or apical process.

⁽H and H') Staining of RG fibers (RC2) in an shRNA-electroporated, radially expanded cerebral cortex (H') revealing the increase and divergence of radial fibers at basal sides upon loss of Tmp1 (radial processes indicated by red dashed lines; reconstruction from two individual confocal images is shown in H') compared to the nonelectroporated hemisphere (H).

⁽I)-(L') Examples of folds observed in the regions electroporated with Trnp1 shRNA at E13 analyzed at E16 (I-J; with I-I" showing rostro-caudal series from the same brain with two independent folds rostrally in I, fusing into a big expanded fold more caudally in I") or postnatal stages (K-L'). Note the macroscopic folds at postnatal stages. Folds are indicated by arrows in (I)-(K) and area with several folds outlined by red arrowheads in (L) and (L'). See also Figures S4 and S5, Table S1, and Movies S1, S2, S3, and S4.

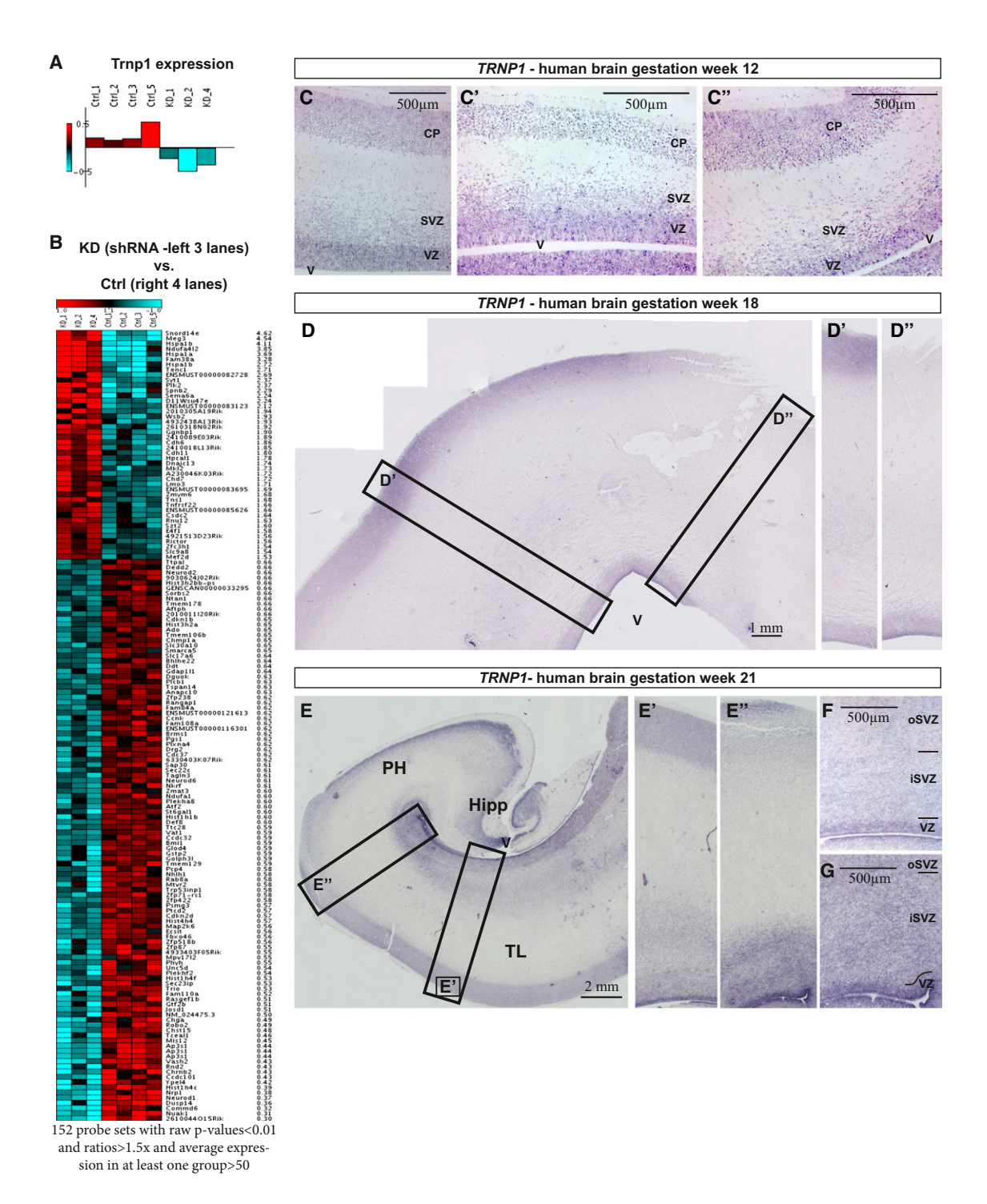


Figure 6. Genome-wide Expression Changes upon Trnp1 Knockdown in Mouse and TRNP1 Expression in Human Cerebral Cortex

(A and B) Heatmap for Trnp1 probe sets (A) and 152 differentially regulated genes (B; average expression >50 in at least one group, p value <0.01, and linear fold change of >1.5-fold) in samples of GFP+ cells sorted by FACS 24 hr after electroporation of E13 cerebral cortex with Trnp1 shRNA (knockdown, KD) or control (Ctrl) constructs.

(C–G) In situ hybridization with *TRNP1* antisense probe of telencephalon sections from human embryos of gws 12 (C–C"), 18 (D–D""), and 21 (E–G). Note the differential expression of *TRNP1* in the VZ of different areas (D', D", E', and E"). (F–G) Zoom of the germinal zones of (E') in (F) and (E") in (G). Hipp, hippocampus; PH, parahippocampal gyrus; TL, temporal lobe.

See also Figures S5 and S6 and Table S2.

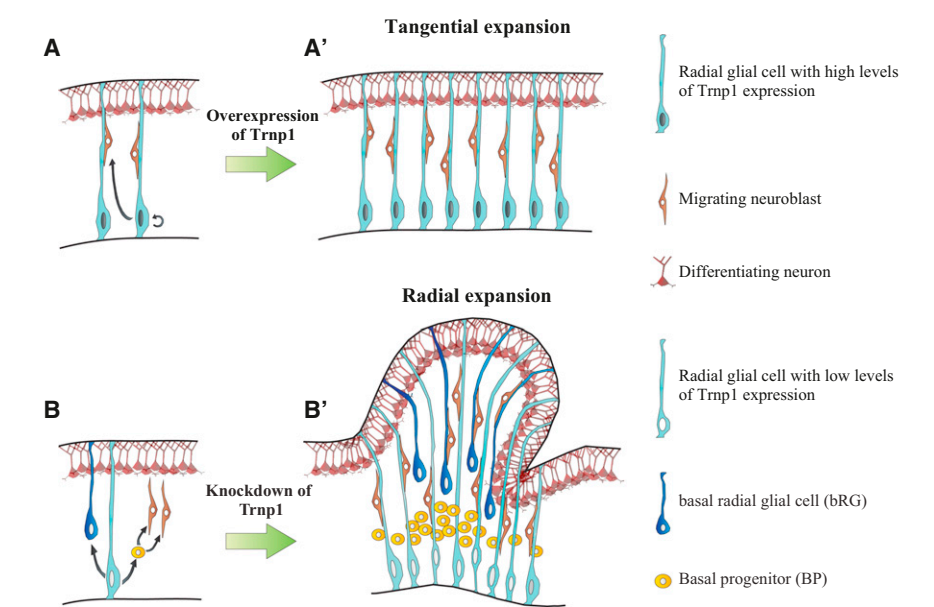


Figure 7. Model of Trnp1 Action in Cerebral **Cortex Development**

Illustration of the function of Trnp1 in NSCs of the developing cerebral cortex.

(A and A') RGs with higher levels of Trnp1 expression (dark-blue nucleus) proliferate and self-renew through either symmetric divisions (generating two RGs) or asymmetric divisions (allowing direct neurogenesis at the same time) (A). Trnp1 overexpression enlarges the pool of apical RGs that self-renew, thereby leading to tangential expansion (A').

(B and B') Apical RGs with lower levels of Trnp1 (empty nucleus) are engaged in the generation of BPs or bRGs (B). Trnp1 knockdown results in a considerable expansion of both BPs and bRG located even beyond the normal SVZ in the mouse cerebral cortex, thereby forming a kind of oSVZ (B'). These concerted changes lead to a radial expansion of the cerebral cortex and ultimately to folding as naturally occurring in species with gyrated cerebral cortices.

oSVZ in species with enlarged cerebral cortex size (Fietz et al., 2010; Hansen et al., 2010; Reillo and Borrell, 2012). This results in considerable radial expansion and simultaneously generates additional radial fibers for lateral dispersion resembling the diverging radial fibers described for gyrencephalic brains by Smart et al. (2002) and Reillo et al. (2011). This provides additional guiding structures for the higher numbers of neurons generated upon Trnp1 knockdown, and we could indeed observe their diverging lateral dispersion during fold formation by live imaging (see Movies S1, S3, and S4). Thus, acute downregulation of Trnp1 is sufficient to regulate the appearance of these hallmarks in a concerted manner, providing an entry point into the cellular and molecular dynamics regulating such complex processes.

Live imaging and genome-wide expression changes upon Trnp1 knockdown allowed us to gain insights into the events leading to these remarkable phenotypes. Trnp1 knockdown had changed the cleavage angles such that more daughter cells lacking an apical anchor were produced, and live imaging confirmed that many more progenitors had delaminated from the apical surface already 24 hr after electroporation of shRNA against Trnp1 compared to controls. Consistent with these cell biological changes, we observed differential expression of molecules involved in apical anchoring of RGs (Table S2), such as Nrp1, Robo2, Cdh6, and Cdh11 (Borrell et al., 2012), and with GTPase activity, such as Trio, a RhoGEF involved in regulating apical constriction (Plageman et al., 2011).

Besides delaminating, cells subject to Trnp1 knockdown actively proliferated at further basal positions of the expanded SVZ, as frequently observed by live imaging for cells with BP or bRG morphology. Again, microarray data revealed a molecular correlate to this behavior because genes promoting the maturation of BPs toward the postmitotic multipolar stage, such as Unc5d, NeuroD1, and NeuroD6 (Miyoshi and Fishell, 2012), were downregulated (Table S2), thereby delaying the progression from the early to the late multipolar stage (LoTurco and Bai, 2006) and maintaining BPs in the proliferative mode for a longer time. Interestingly, these genes are also regulated by FoxG1 (Miyoshi and Fishell, 2012), whose expression resembles Trnp1 in as much as it is also high in VZ progenitors, then expression is reduced in SVZ progenitors but increased in postmitotic neurons.

Finally, live imaging also revealed an indication of a possible role of Trnp1 in postmitotic neurons because their migration was much faster when Trnp1 levels were reduced (Movie S1 as compared to Movie S2) in correlation with downregulation of proteins involved in regulating neuronal migration (Table S2). Consistent with its endogenous expression, Trnp1 knockdown affected gene expression at various stages in the lineage progression from VZ to SVZ progenitors and differentiating neurons (Table S2). Hence, Trnp1 affects all of these steps in a concerted manner thereby coordinating cellular behaviors that ultimately result in considerable radial expansion and gyrus formation in the cerebral cortex.

Phylogenetic Consideration

This striking phenotype raised the question of to what extent Trnp1 is relevant to regulating gyrification during phylogeny. The degree of cortical gyrification across phylogeny has been shown to correlate positively with the abundance of bRG. Because almost all mammalian superorders comprise species with smooth lissencephalic brains and also folded gyrencephalic brains, regulatory mechanisms may presumably be present in all mammals (Borrell and Reillo, 2012; Kelava et al., 2012; García-Moreno et al., 2012). Rather than the invention of a "new" gene in gyrencephalic mammals, such preexisting genes may have been co-opted via their differential regulation (True and Carroll, 2002). Our findings showing that Trnp1 levels regulate the proportion of BPs and bRGs simultaneously support this hypothesis and provide a mechanistic basis for the finding that the proportion of bRGs and the extent of gyrification have changed several times during mammalian evolution (Borrell and Reillo, 2012; Kelava et al., 2012). Such mechanisms may also explain the selective expansion of some areas of the cerebral cortex. As a first step toward elucidating these fascinating questions, we show here that *TRNP1* is also expressed in the VZ and neuronal layers of the developing human cerebral cortex, and quantitative differences in *TRNP1* expression seemingly correlate with some of the regions undergoing more or less folding.

Our findings thus unraveled Trnp1 as a molecular factor involved in the regulation of both tangential and radial expansion of the cerebral cortex. This shows that the dynamic regulation of the expression of a single gene is sufficient to orchestrate the events required for gyrus formation even in a naturally lissence-phalic cerebral cortex. Manipulations of Trnp1 levels further support a model by which dynamic regulation of one factor can contribute to differential expansion of distinct cortical regions controlling first tangential and then radial expansion of a given neocortical region. This scenario therefore provides a blueprint to study the cellular and molecular mechanisms of cerebral cortex expansion and folding.

EXPERIMENTAL PROCEDURES

Immunostaining, in utero electroporation, dissociated cell cultures, in situ hybridization, and retrovirus production were performed as described previously (Cappello et al., 2012; Flames et al., 2007) and are also available in detail in the Extended Experimental Procedures. All experimental procedures were performed in accordance with the regulations of the Helmholtz Center Munich, and animal experiments were approved by the government of upper Bavaria.

Plasmid Constructs

The coding sequence of *Tmp1* was subcloned from pCMV-Sport6-*Tmp1* (RZPD clone) into pCAG-GFP and pCAG-dsRed (pCAG destination vectors were a kind gift of Paolo Malatesta). To downregulate Trnp1 expression, three different shRNAs were cloned into pSUPER.GFP/Neo: shRNA #1, 5′-ACTCTGCATTGCTTCCCATACACTG-3′; shRNA #4, 5′-GCAGAAAGG CAAGCCACTTCT-3′; and shRNA #5, 5′-GATGGACGGCGTCATCTAC-3′, each targeting different regions of the 3′ UTR of *Tmp1-mRNA*. The target region is not contained in the pCAG-*Tmp1*-GFP/dsRed vector which was therefore usable for rescue of the knockdown effect. Empty pCAG-GFP, pCAG-dsRed, and pSUPER-GFP.Neo vectors were used as controls. For detailed cloning strategy, see the Extended Experimental Procedures.

Human Tissue

Brain sections of human fetuses from spontaneous abortions were obtained from the Service of Pathology, Hospital Universitario Principe de Asturias, Alcalá de Henares, Spain. Brains were removed in routine necropsies in accordance with the Spanish law on clinical autopsies (Boletín Oficial del Estado [BOE] June 27, 1980, and BOE September 11, 1982). After removal, brains were fixed by immersion in buffered 4% paraformaldehyde (PFA) at room temperature during 2 weeks. Then coronal blocks across the entire brain were obtained; these blocks were embedded in toto in paraffin and finally sectioned and stained. For additional methods, please see the Extended Experimental Procedures.

ACCESSION NUMBERS

Array data have been submitted to GEO (record GSE40582), and the following link allows review while it remains in private status: http://www.ncbi.nlm.nih.gov/geo/query/acc.cgi?token=tzcrzsuwmecogbu&acc=GSE40582.

SUPPLEMENTAL INFORMATION

Supplemental Information includes Extended Experimental Procedures, six figures, two tables, and four movies and can be found with this article online at http://dx.doi.org/10.1016/j.cell.2013.03.027.

ACKNOWLEDGMENTS

We are particularly grateful to Gabriele Jäger, Andrea Steiner-Mezzadri, and Emily Violette Baumgart for excellent technical support and to Alexandra Lepier and Simone Bauer for support in regard to viral vector production. We thank Judith Fischer-Sternjak for help with flow cytometry. Particular thanks to Atsunori Shitamukai and Fumio Matsuzaki for the constructs used for electroporation to visualize the morphology of basal radial glial cells by live imaging. We also thank Paolo Malatesta for the pCAG destination vectors. Special thanks to Olga Díez Jambrina (Service of Pathology, Hospital Universitario Principe de Asturias, Alcalá de Henares, Spain) for invaluable help in processing the tissue from human fetal brains and to Wolfgang Enard for great discussions and very helpful comments on the manuscript. This work was funded by MICINN with a "Juan de la Cierva" contract to C.D.J.R. and grants SAF2009-07367 and CONSOLIDER CSD2007-00023 to V.B., and by the DFG via the Gottfried-Wilhelm Leibniz Award, the German Excellence Program (LMU Excellent, CIPS), and the SFB 870 to M.G.

Received: October 8, 2012 Revised: January 31, 2013 Accepted: March 13, 2013 Published: April 25, 2013

REFERENCES

Asami, M., Pilz, G.A., Ninkovic, J., Godinho, L., Schroeder, T., Huttner, W.B., and Götz, M. (2011). The role of Pax6 in regulating the orientation and mode of cell division of progenitors in the mouse cerebral cortex. Development 138. 5067–5078.

Bayatti, N., Moss, J.A., Sun, L., Ambrose, P., Ward, J.F.H., Lindsay, S., and Clowry, G.J. (2008). A molecular neuroanatomical study of the developing human neocortex from 8 to 17 postconceptional weeks revealing the early differentiation of the subplate and subventricular zone. Cereb. Cortex 18, 1536–1548.

Borrell, V., and Reillo, I. (2012). Emerging roles of neural stem cells in cerebral cortex development and evolution. Dev. Neurobiol. 72, 955–971.

Borrell, V., Cárdenas, A., Ciceri, G., Galcerán, J., Flames, N., Pla, R., Nóbrega-Pereira, S., García-Frigola, C., Peregrín, S., Zhao, Z., et al. (2012). Slit/Robo signaling modulates the proliferation of central nervous system progenitors. Neuron 76. 338–352.

Cappello, S., Böhringer, C.R.J., Bergami, M., Conzelmann, K.-K., Ghanem, A., Tomassy, G.S., Arlotta, P., Mainardi, M., Allegra, M., Caleo, M., et al. (2012). A radial glia-specific role of RhoA in double cortex formation. Neuron *73*, 911–924

Chenn, A., and Walsh, C.A. (2002). Regulation of cerebral cortical size by control of cell cycle exit in neural precursors. Science 297, 365–369.

Costa, M.R., Wen, G., Lepier, A., Schroeder, T., and Götz, M. (2008). Par-complex proteins promote proliferative progenitor divisions in the developing mouse cerebral cortex. Development *135*, 11–22.

Dehay, C., and Kennedy, H. (2007). Cell-cycle control and cortical development. Nat. Rev. Neurosci. 8, 438–450.

Farkas, L.M., Haffner, C., Giger, T., Khaitovich, P., Nowick, K., Birchmeier, C., Pääbo, S., and Huttner, W.B. (2008). Insulinoma-associated 1 has a panneurogenic role and promotes the generation and expansion of basal progenitors in the developing mouse neocortex. Neuron 60, 40–55.

Fietz, S.A., and Huttner, W.B. (2011). Cortical progenitor expansion, self-renewal and neurogenesis—a polarized perspective. Curr. Opin. Neurobiol. *21*, 23–35.

Fietz, S.A., Kelava, I., Vogt, J., Wilsch-Bräuninger, M., Stenzel, D., Fish, J.L., Corbeil, D., Riehn, A., Distler, W., Nitsch, R., and Huttner, W.B. (2010). OSVZ progenitors of human and ferret neocortex are epithelial-like and expand by integrin signaling. Nat. Neurosci. 13, 690-699.

Fish, J.L., Dehay, C., Kennedy, H., and Huttner, W.B. (2008). Making bigger brains-the evolution of neural-progenitor-cell division. J. Cell Sci. 121, 2783-

Flames, N., Pla, R., Gelman, D.M., Rubenstein, J.L., Puelles, L., and Marín, O. (2007). Delineation of multiple subpallial progenitor domains by the combinatorial expression of transcriptional codes. J. Neurosci. 27, 9682-9695.

García-Moreno, F., Vasistha, N.A., Trevia, N., Bourne, J.A., and Molnár, Z. (2012). Compartmentalization of cerebral cortical germinal zones in a lissencephalic primate and gyrencephalic rodent. Cereb. Cortex 22, 482-492.

Götz, M., and Huttner, W.B. (2005). The cell biology of neurogenesis. Nat. Rev. Mol. Cell Biol. 6, 777-788.

Hansen, D.V., Lui, J.H., Parker, P.R.L., and Kriegstein, A.R. (2010). Neurogenic radial glia in the outer subventricular zone of human neocortex. Nature 464, 554-561

Haubensak, W., Attardo, A., Denk, W., and Huttner, W.B. (2004). Neurons arise in the basal neuroepithelium of the early mammalian telencephalon: a major site of neurogenesis. Proc. Natl. Acad. Sci. USA 101, 3196-3201.

Haubst, N., Berger, J., Radjendirane, V., Graw, J., Favor, J., Saunders, G.F., Stoykova, A., and Götz, M. (2004). Molecular dissection of Pax6 function: the specific roles of the paired domain and homeodomain in brain development. Development 131, 6131-6140.

Heinrich, C., Gascón, S., Masserdotti, G., Lepier, A., Sanchez, R., Simon-Ebert, T., Schroeder, T., Götz, M., and Berninger, B. (2011). Generation of subtype-specific neurons from postnatal astroglia of the mouse cerebral cortex. Nat. Protoc. 6, 214-228.

Kelava, I., Reillo, I., Murayama, A.Y., Kalinka, A.T., Stenzel, D., Tomancak, P., Matsuzaki, F., Lebrand, C., Sasaki, E., Schwamborn, J.C., et al. (2012). Abundant occurrence of basal radial glia in the subventricular zone of embryonic neocortex of a lissencephalic primate, the common marmoset Callithrix jacchus. Cereb. Cortex 22, 469-481.

Kooistra, S.M., van den Boom, V., Thummer, R.P., Johannes, F., Wardenaar, R., Tesson, B.M., Veenhoff, L.M., Fusetti, F., O'Neill, L.P., Turner, B.M., et al. (2010). Undifferentiated embryonic cell transcription factor 1 regulates ESC chromatin organization and gene expression. Stem Cells 28, 1703-1714.

Krubitzer, L. (2007). The magnificent compromise: cortical field evolution in mammals. Neuron 56, 201-208.

LoTurco, J.J., and Bai, J. (2006). The multipolar stage and disruptions in neuronal migration. Trends Neurosci. 29, 407-413.

Lui, J.H., Hansen, D.V., and Kriegstein, A.R. (2011). Development and evolution of the human neocortex. Cell 146, 18-36.

Martínez-Cerdeño, V., Cunningham, C.L., Camacho, J., Antczak, J.L., Prakash, A.N., Cziep, M.E., Walker, A.I., and Noctor, S.C. (2012). Comparative analysis of the subventricular zone in rat, ferret and macaque: evidence for an outer subventricular zone in rodents. PLoS One 7, e30178.

Miyoshi, G., and Fishell, G. (2012). Dynamic FoxG1 expression coordinates the integration of multipolar pyramidal neuron precursors into the cortical plate. Neuron 74, 1045-1058.

Pinto, L., Mader, M.T., Irmler, M., Gentilini, M., Santoni, F., Drechsel, D., Blum, R., Stahl, R., Bulfone, A., Malatesta, P., et al. (2008). Prospective isolation of functionally distinct radial glial subtypes-lineage and transcriptome analysis. Mol. Cell. Neurosci. 38, 15-42.

Pinto, L., Drechsel, D., Schmid, M.T., Ninkovic, J., Irmler, M., Brill, M.S., Restani, L., Gianfranceschi, L., Cerri, C., Weber, S.N., et al. (2009). AP2γ regulates basal progenitor fate in a region- and layer-specific manner in the developing cortex. Nat. Neurosci. 12, 1229-1237.

Plageman, T.F., Jr., Chauhan, B.K., Yang, C., Jaudon, F., Shang, X., Zheng, Y., Lou, M., Debant, A., Hildebrand, J.D., and Lang, R.A. (2011). A Trio-RhoA-Shroom3 pathway is required for apical constriction and epithelial invagination. Development 138, 5177-5188.

Rakic, P. (1995). A small step for the cell, a giant leap for mankind: a hypothesis of neocortical expansion during evolution. Trends Neurosci. 18, 383-388.

Reillo, I., and Borrell, V. (2012). Germinal zones in the developing cerebral cortex of ferret: ontogeny, cell cycle kinetics, and diversity of progenitors. Cereb. Cortex 22, 2039-2054.

Reillo, I., de Juan Romero, C., García-Cabezas, M.A., and Borrell, V. (2011). A role for intermediate radial glia in the tangential expansion of the mammalian cerebral cortex. Cereb. Cortex 21, 1674-1694.

Shitamukai, A., Konno, D., and Matsuzaki, F. (2011). Oblique radial glial divisions in the developing mouse neocortex induce self-renewing progenitors outside the germinal zone that resemble primate outer subventricular zone progenitors. J. Neurosci. 31, 3683-3695.

Smart, I.H.M., Dehay, C., Giroud, P., Berland, M., and Kennedy, H. (2002). Unique morphological features of the proliferative zones and postmitotic compartments of the neural epithelium giving rise to striate and extrastriate cortex in the monkey. Cereb. Cortex 12, 37-53.

True, J.R., and Carroll, S.B. (2002). Gene co-option in physiological and morphological evolution. Annu. Rev. Cell Dev. Biol. 18, 53-80.

van den Boom, V., Kooistra, S.M., Boesjes, M., Geverts, B., Houtsmuller, A.B., Monzen, K., Komuro, I., Essers, J., Drenth-Diephuis, L.J., and Eggen, B.J.L. (2007). UTF1 is a chromatin-associated protein involved in ES cell differentiation. J. Cell Biol. 178, 913-924.

Volpe, M., Shpungin, S., Barbi, C., Abrham, G., Malovani, H., Wides, R., and Nir, U. (2006). trnp: a conserved mammalian gene encoding a nuclear protein that accelerates cell-cycle progression. DNA Cell Biol. 25, 331-339.

Wang, X., Tsai, J.W., LaMonica, B., and Kriegstein, A.R. (2011). A new subtype of progenitor cell in the mouse embryonic neocortex. Nat. Neurosci. 14, 555-561.

Note Added in Proof

A recent paper by Nonaka-Kinoshita et al. in EMBO J describes effects on gyrification in the ferret cerebral cortex by altering cell-cycle properties, although this is not sufficient to achieve gyrification in mouse cerebral cortex. Nonaka-Kinoshita, M., Reillo, I., Artegiani, B., Martínez-Martínez, M.A., Nelson, M., Borrell, V., and Calegari, F. (2013). Regulation of cerebral cortex size and folding by expansion of basal progenitors. Published online April 26, 2013. http://dx.doi.org/10.1038/emboj.2013.96.

Supplemental Information

EXTENDED EXPERIMENTAL PROCEDURES

Animals

C57BL/6J wild-type mice were bred in the animal facility of the Helmholtz-Center Munich and the day of the vaginal plug was considered embryonic day (E) 0. All experimental procedures were performed in accordance with German and European Union guidelines.

Quantitative Analysis

Single optical sections (confocal microscopy) of each brain slice were analyzed in a 200 µm thick radial stripe for GFP, BrdU, Pax6 and Tbr2 positive cells. For bRG quantifications, Pax6+ cells outside of the Tbr2+ dense cellular band (typically more than 200 µm away from apical surface) were quantified. Quantifications are given as mean +/- SEM. Different sections representing the full rostrocaudal distribution of the electroporated area were used for quantifications of each condition. For the overexpression analysis (pCAG-GFP versus pCAG-Trnp1-GFP) more than 4000 cells were quantified from 5 different embryos (from 3-4 different litters) for each control and overexpression. For the knockdown analysis (pSUPER.GFP/Neo versus pSUPER.GFP/Neo-shRNA) more than 3500 cells were quantified from 5 different embryos (from 2-4 different litters) for each control, knockdown and rescue experiments.

For the in-vitro clonal analysis, clone size and clone composition of each clone was determined and the mean was calculated per experiment with 4 independent experiments (5 coverslips per experiment, with less than 25 clones each).

Statistical significance was tested using nonparametric Mann-Whitney U-Test (also called Wilcoxon rank-sum test or Mann-Whitney-Wilcoxon (MWW) test) in case of in vivo studies and ANOVA with a Tukey's posthoc test or Students t test in the case of in vitro studies. P values less than 0.05 were considered significant.

Immunostainings

Embryonic brains were fixed for 1.5-6 hr (h) (E10/E12: 1,5 h; E14: 2 h; E16/E16,5: 4 h; E18: 6 h) in 4% Paraformaldehyde (PFA) (in PBS) with gentle rotation at 4°C. Brains were then cryoprotected in 30% sucrose (in PBS) overnight, embedded in tissue-tek, stored at -20°C and then cryosectioned (12-30 μm). Cell cultures were fixed in 4% PFA for 15 min and washed with PBS. Sections or cells on coverslips were blocked with 2%BSA, 0.5% Triton (in PBS) for 1h prior to staining. Primary antibodies were applied in blocking solution overnight at 4°C (cryosections) or for 2h at room temperature (for coverslips). Primary antibodies were: anti-Trnp1 (guinea pig, raised against: AETPVEGQELQRWRQGASG, Peptide specialty Laboratories Heidelberg, 1:200), anti-Pax6 (rabbit, Millipore, 1:200; mouse, Dev. Hybridoma Bank, 1:50), anti-Tbr2 (rabbit, Abcam, 1:500), anti-TBR1 (rabbit, Millipore, 1:100), anti-GFP (chicken, Aves Labs, 1:1000), anti-BrdU (rat, Abcam, 1:400), anti-RC2 (mouse IgGM, Dev. Hybridoma Bank, 1:200), anti-βIII Tubulin (mouse IgG2b, Sigma, 1:500), anti-RFP (mlgG2a, Chromotek, 1:200). Fluorescent secondary antibodies were applied according to the manufacturer's protocol (Jackson or Molecular Probes). To visualize nuclei, sections were incubated for 10 min in 0.1 µg/ml DAPI (4'.6-Diamidin-2-phenylindol, Sigma). Sections were mounted in Aqua Polymount (Polysciences). Stainings were analyzed using Zeiss (LSM710) or Leica (SP5) laser-scanning microscopes. Alternatively, AxioImager.M2 and AxioVision MosaiX software was used for overviews. For staining of Trnp1 or BrdU, sections were pretreated with 2N HCl for 30 min and subsequently neutralized with sodium-tetraborate (Na₂B₄O₇ 0.1M, pH: 8.5) for 2×15 min.

Plasmid Constructs

We cloned the coding sequence of Trnp1 from pCMV-Sport6-Trnp1 (RZPD clone) into a Gateway (Invitrogen) form of pCAG-GFP and pCAG-dsRed (pCAG destination vectors kind gift of Paolo Malatesta). For that purpose, we first removed the poly-A signal and parts of the 3'-UTR from the initial pCMV-Sport6-Trnp1 expression clone by BamHI/Xbal digestion, reblunting and relegation. We then cloned Trnp1 cDNA into pENTR1A via EcoRI/Xhol and finally via a Gateway LR-reaction into the pCAG destination vectors.

For knock down of Trnp1 we designed five different shRNA sequences with the help of BlockIT (Invitrogen) or oligoengine software. Three of these shRNA sequences were cloned into pSUPER.GFP/Neo according to the manufacturer's protocol (Oligoengine): shRNA#1: 5'-ACTCTGCATTGCTTCCCATACACTG-3'; shRNA#4: 5'-GCAGAAAGGCAAGCCACTTCT-3' and shRNA#5: 5'-GATG GACGGCGTCATCTAC-3'. Each of them target different regions within the 3'-UTR of Trnp1 that are not contained in the pCAG-Trnp1-GFP/dsRed vector (see above). Therefore pCAG-Trnp1-dsRed was also used to rescue the knock down effect of shRNAs. All of the mentioned constructs were verified by DNA sequencing. All plasmids were produced under endotoxin free conditions (QIAGEN EndoFree Plasmid Maxi Kit). Empty pCAG-GFP, pCAG-dsRed and pSUPER-GFP.Neo vectors were used as controls.

Retrovirus Production

Replication incompetent MMLV based, VSV-G pseudotyped retroviruses of the different pCAG constructs (see above) were produced in GPG-293 packaging cells (Ory et al., 1996) as described previously (Heinrich et al., 2011). Estimation of the viral titer was performed as previously described (Hack et al., 2005) resulting in a typical titer of 5x10⁷/ml.

Dissociated Cell Cultures of the Embryonic Cerebral Cortex

Brains were isolated from embryos of E14 timed pregnant C57BL/6 wild-type mice. Cortices were dissected and pooled in HBSS buffer with 10mM HEPES. Cortical cells were enzymatically dissociated using 0.05% Trypsin/EDTA for 15 min at 37°C with subsequent resuspension of cells in DMEM containing 10% fetal calf serum (FCS) to stop the enzymatic reaction. Then, a fire polished Pasteur pipette, preincubated in DMEM/FCS to coat the glass was used to mechanically dissociate the cells. Primary cortical cells were plated at a density of 2.5×10^5 cells / well (of a 24 well plate) and infected with a low viral titer (<25 particles) 2h later. Medium changes and fixation after 7 days in vitro were performed as described previously (Heins et al., 2001). A clear separation of clones - each derived from a single cell - could be achieved as described previously (Williams et al., 1991; Haubst et al., 2004; Costa et al., 2008) by using a low number of viral particles (<25 clones per well).

Time-Lapse Imaging of Dissociated Cell Cultures of the Embryonic Cerebral Cortex

Time-lapse video microscopy and single cell tracking of dissociated cultures from the embryonic cerebral cortex at E14 was performed as described previously (Costa et al., 2008; Eilken et al., 2009; Schroeder, 2011) with a cell observer (Zeiss) at a constant temperature of 37°C and 8% CO₂. Phase contrast images were acquired every 5 min for 6-8 days using a 20x phase contrast objective (Zeiss), an AxioCamHRm camera and a Zeiss AxioVision 4.7 software. Single-cell tracking was performed using a self-written computer program (TTT) (Rieger et al., 2009). Movies were assembled using Image J 1.42q (National Institute of Health, USA) software.

In Utero Electroporation

Animals were operated as approved by the Government of Upper Bavaria under license number 55.2-1-54-2531-144/07 and number 55.2-1-54-2532-79/11. E13 timed pregnant mice were anaesthetized by intraperitoneal (i.p.) injection of Fentanyl (0.05mg/kg), Midazolam (5mg/kg) and Medetomidine (0.5mg/kg) (Btm license number: 4518395). Plasmids were mixed with Fast Green ($2.5mg/\mu l$, Sigma) and injected at a concentration of $1 \mu g/\mu l$. In utero electroporations were done as described earlier (Saito, 2006). Anesthesia was terminated by subcutaneous injection of Buprenorphine (0.1mg/kg), Atipamezol (2.5mg/kg), Flumazenil (0.5mg/kg). Embryonic brains were fixed and sliced as described above.

Time-Lapse Imaging of Slice Cultures

For imaging either pCAG-GFP alone or p.SUPER-shRNA#1 together with pCAG-GFP were coelectroporated at a final concentration of $1\mu g/\mu l$ together with Fast Green ($2.5\mu g/\mu l$; Sigma) (Movies S1, S2, and S3). To achieve more sparse labeling and detailed information about cell morphology the plasmids pSUPER-shRNA#1 ($0.5\mu g/\mu l$), pCAG-Floxp-EGFP-N1 and pCAG-Floxp-mKO2-F (both $0.5-0.8\mu g/\mu l$) were coelectroporated together with a low concentration of pCAG-Cre ($0.5-1ng/\mu l$) to achieve clonal labeling of progenitor cells as described previously by Shitamukai et al. (2011).

Slices of electroporated cerebral cortices were prepared and imaged as described previously (Shitamukai et al., 2011). Slices were cut at 300 µm thickness on a vibratome (Leica VT 1200). The time interval between each time point taken was 30 min.

Acidic Extraction of DNA-Associated Molecules

Nuclei were first prepared by resuspending the cellular pellet in 3 volumes of HRSB – 0.5% NP40 (20 mM HEPES pH 7.6, 3 mM MgCl2, 10 mM NaCl, 0.5% NP40). Nuclei suspension was sedimented on a 1 ml HRSB-Sucrose (1.2M) gradient (centrifuged for 5 min at 2400 g at 4°C) and reconstituted in 10 pellet volumes Extraction – EDTA buffer (10 mM HEPES pH 7.6, 150 mM NaCl, 1 mM EDTA, 10% glycerol, add 1 mM DTT). Supernatant was kept and labeled as washing fraction. For acidic extraction, the pellet was resuspended in 10 pellet volumes ice-cold 0.4 M HCl and kept on ice for 1 hr. Samples were vortexed every 15 min during the 1 hr incubation time. Samples were centrifuged for 10 min at 13 000 rpm and supernatant (acid supernatant containing most of DNA bound molecules) was collected. 8 volumes of acetone were added to the pellet, mixed and then stored at -20° C overnight. The next day, acetone pellets were centrifuged at 4600 rpm for 10 min at 4°C and pellets were washed with 0.5 ml acetone (-20° C), spun at 4600 rpm for 5 min. The pellet was dried and resuspended in 100 μ l SDS loading buffer. Nuclei, washing fraction, acidic supernatant and acidic pellet were separated by SDS PAGE and western blotting was performed to detect the protein of interest.

cRNA Probe Synthesis and In Situ Hybridization of Human TRNP1

Human *TRNP1* in pOTB7 was obtained from "Source BioScience LifeSciences." The insert was sequenced using M13 forward primer. Nonradioactive cRNA probes were produced with digoxigenin (DIG) (Roche Diagnostics, Mannheim, Germany) according to the manufacturer's instructions. The linearized plasmids were transcribed with T7 or SP6 RNA polymerase (New England Biolabs, Ipswich, MA) followed by labeling with digoxigenin to generate sense and antisense probes. Probes were purified by NaAC 3M/EtOH precipitation. Correct probe size was verified by formaldehyde-agarose gel electrophoresis. In situ hybridization was performed as described elsewhere (Flames et al., 2007). Paraffin sections of 5 μm thickness were de-paraffined, (post-) fixed with 4% formaldehyde in PBS and pretreated with proteinase K. Sections were hybridized with cRNA probes at a final concentration of 200 – 400 ng/ml overnight at 58°C in hybridization solution [50% formamide (Ambion, Austin, TX), 10% dextran sulfate, 0.2% tRNA (Invitrogen, Carlsbad, CA), 1x Denhardts solution (from a 50x stock; Sigma, St. Louis, MO), 1x salt solution (containing 0.2 M NaCl, 0.01 M Tris, 5 mM NaH₂PO₄, 5 mM Na₂HPO₄, 5 mM EDTA, pH 7.5)]. After the sections were washed, alkaline phosphatase-coupled anti-digoxigenin Fab fragments were applied. For visualization of the labeled cRNAs, the sections were incubated in the dark in nitroblue tetrazolium (NBT)/5-bromo-4-chloro-3-indolyl phosphate (BCIP) solution [3.4 μl/ml from NBT stock and 3.5 μl/ml from BCIP stock in reaction buffer (100 mg/ml NBT stock in 70% dimethylformamide; 50 mg/ml BCIP stock in 100% dimethylformamide; Roche)].

FACS

Cortices from E14 embryos electroporated 24 hr earlier (at E13 with either shRNA plasmid or control plasmid) were dissected removing the ganglionic eminence, the olfactory bulb, the hippocampal anlage and the meninges. Cortices from each litter were pooled and cells were enzymatically dissociated and resuspended in PBS. GFP positive cells were isolated using the FACSArialII (BD Bioscience) system at purity mode and a flow rate lower than 1200 cells per second for high purity. Forward- and sideward scatter were adjusted to exclude cell debris and include only GFP positive cells that were detected by 488nm laser-assisted excitation. Gating for GFP fluorescent cells was set using WT cortical cells from nonelectroporated embryos. Cells were directly sorted into RLT (QIAGEN) buffer to enhance RNA quality and efficiency.

Microarray Analysis

RNA was isolated from the above described FACS sorted cells using the RNeasy Micro kit (QIAGEN) or RNeasy Mini kit (QIAGEN) according to the manufacturer's instructions including digestion of remaining genomic DNA. For microarray analysis RNA concentration and quality was measured using an Agilent 2100 Bioanalyzer. RIN values of the samples ranged from 8.0 to 10. For each microarray approximately 0.5 - 2 ng of RNA per experiment was first amplified using the "Ovation PicoSL WTA System V2" kit in combination with the Encore Biotin Module (Nugen). Then, 2.1 µg of amplified cDNA were hybridized on Affymetrix Gene ST 1.0 arrays (containing about 28.000 probe sets) according to the manufacturer's instructions. Expression console software (v.1.2. Affymetrix) was used for quality control and to obtain annotated normalized RMA gene-level data (standard settings including sketch-quantile normalization). The statistical analysis of the microarray data was performed by utilizing the statistical programming environment (R Development Core Team, 2005) implemented in CARMAweb (Rainer et al., 2006). Significantly (p<0.01) regulated genes were further filtered for average expression > 50 in at least one group (knockdown or control) and for linear ratios > 1.5x (KD / Ctrl). Heatmaps were generated with CARMAweb and GO term and pathway enrichment analyses (p<0.01) were done with GePS software (Genomatix, Germany).

SUPPLEMENTAL REFERENCES

Eilken, H.M., Nishikawa, S.-I., and Schroeder, T. (2009). Continuous single-cell imaging of blood generation from haemogenic endothelium. Nature 457, 896–900. Hack, M.A., Saghatelyan, A., de Chevigny, A., Pfeifer, A., Ashery-Padan, R., Lledo, P.-M., and Götz, M. (2005). Neuronal fate determinants of adult olfactory bulb neurogenesis. Nat. Neurosci. 8, 865-872.

Heins, N., Cremisi, F., Malatesta, P., Gangemi, R.-M., Corte, G., Price, J., Goudreau, G., Gruss, P., and Götz, M. (2001). Emx2 promotes symmetric cell divisions and a multipotential fate in precursors from the cerebral cortex. Mol. Cell. Neurosci. 18, 485-502.

Ory, D.S., Neugeboren, B.A., and Mulligan, R.C. (1996). A stable human-derived packaging cell line for production of high titer retrovirus/vesicular stomatitis virus G pseudotypes. Proc. Natl. Acad. Sci. USA 93, 11400-11406.

R Development Core Team. (2005). R: a language and environment for statistical computing. R Foundation for Statistical Computing, Vienna. ISBN 3-900051-07-0, http://www.r-project.org.

Rainer, J., Sanchez-Cabo, F., Stocker, G., Sturn, A., and Trajanoski, Z. (2006). CARMAweb: comprehensive R- and bioconductor-based web service for microarray data analysis. Nucleic Acids Res. 34(Web Server issue), W498–W503.

Rieger, M.A., Hoppe, P.S., Smejkal, B.M., Eitelhuber, A.C., and Schroeder, T. (2009). Hematopoietic cytokines can instruct lineage choice. Science 325, 217–218. Saito, T. (2006). In vivo electroporation in the embryonic mouse central nervous system. Nat. Protoc. 1, 1552–1558.

Schroeder, T. (2011). Long-term single-cell imaging of mammalian stem cells. Nat. Methods 8(4, Suppl), S30-S35.

Williams, B.P., Read, J., and Price, J. (1991). The generation of neurons and oligodendrocytes from a common precursor cell. Neuron 7, 685-693.

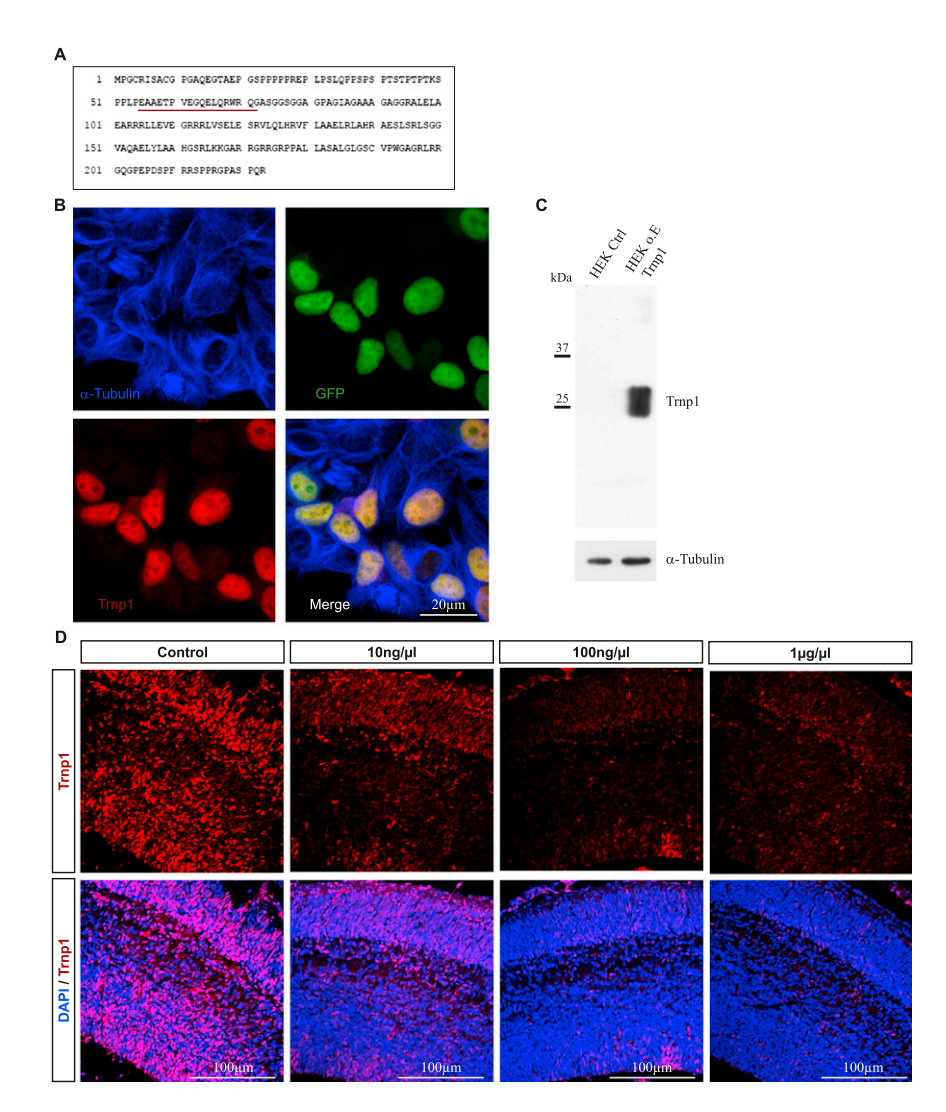


Figure S1. Analysis of the Specificity of Anti-Trnp1 Antibody and Trnp1 Localization in the Adult Brain, Related to Figure 1

(A) depicts the protein sequence of Trnp1 with the sequence of 19 amino acids against which the antibody was raised underlined in red (aa 57 - aa 75). (B and C) Immunocytochemistry and western blotting upon overexpression of Trnp1 or a Trnp1-GFP fusion protein in HEK cells devoid of endogenous Trnp1 protein confirmed the specificity of the antibody. (B) Immunocytochemistry of HEK293 cells transiently transfected with peGFP-N3-Tmp1 to express a Trnp1-GFP fusion protein. Cells were fixed 48h posttransfection. Localization of the fusion protein was visualized by GFP staining. To visualize the cytoplasm of the cells staining for α-tubulin was performed. Additionally, Trnp1 expression was directly visualized with the antibody generated against Trnp1 as depicted in A. The merge confirmed the specificity of the Trnp1 antibody and showed that the protein is exclusively localized in the nucleus. Note that only transfected cells showed Trnp1 expression three days after transfection. Single optical sections are shown. (C) Western blot of HEK cells transfected with pCMV-Trnp1 for overexpression of Trnp1. Note that no signal can be detected in untransfected HEK cells.

(D) We further tested the specificity of the antibody by immunostaining on brain sections and competing with antibody antigen interaction using increasing concentrations of the 19 amino acid peptide against which the antibody was raised. Immunohistochemistry of E14 coronal sections is shown. Sections were stained with Trnp1 antibody preincubated with different concentrations (as indicated) of the peptide used for generation of the antibody. Note that higher concentrations of the peptide were able to block the nuclear signal of immunohistochemistry.

(E-H) Sagittal sections of the adult murine brain labeled for Trnp1, DAPI and Dcx or BrdU (single optical sections are shown). (E) depicts Trnp1 immunostaining in the adult subependymal zone (SEZ), rostral migratory stream (RMS) and the olfactory bulb (OB) glomerular layer (GL) or granular cell layer (GCL). (F) Overview of Trnp1 and Dcx (neuroblasts) colabeling in the SEZ and the RMS. (G) Trnp1 and Dcx or BrdU (BrdU treatment 1h prior to sacrifice) colabeling in the SEZ. Note that Dcx positive neuroblasts and all transit amplifying (BrdU positive, but Dcx-negative) progenitors are Trnp1-immunoreactive. (H) Trnp1 immunostaining is absent in the dentate gyrus. LV: lateral ventricle; scale bars as indicated.

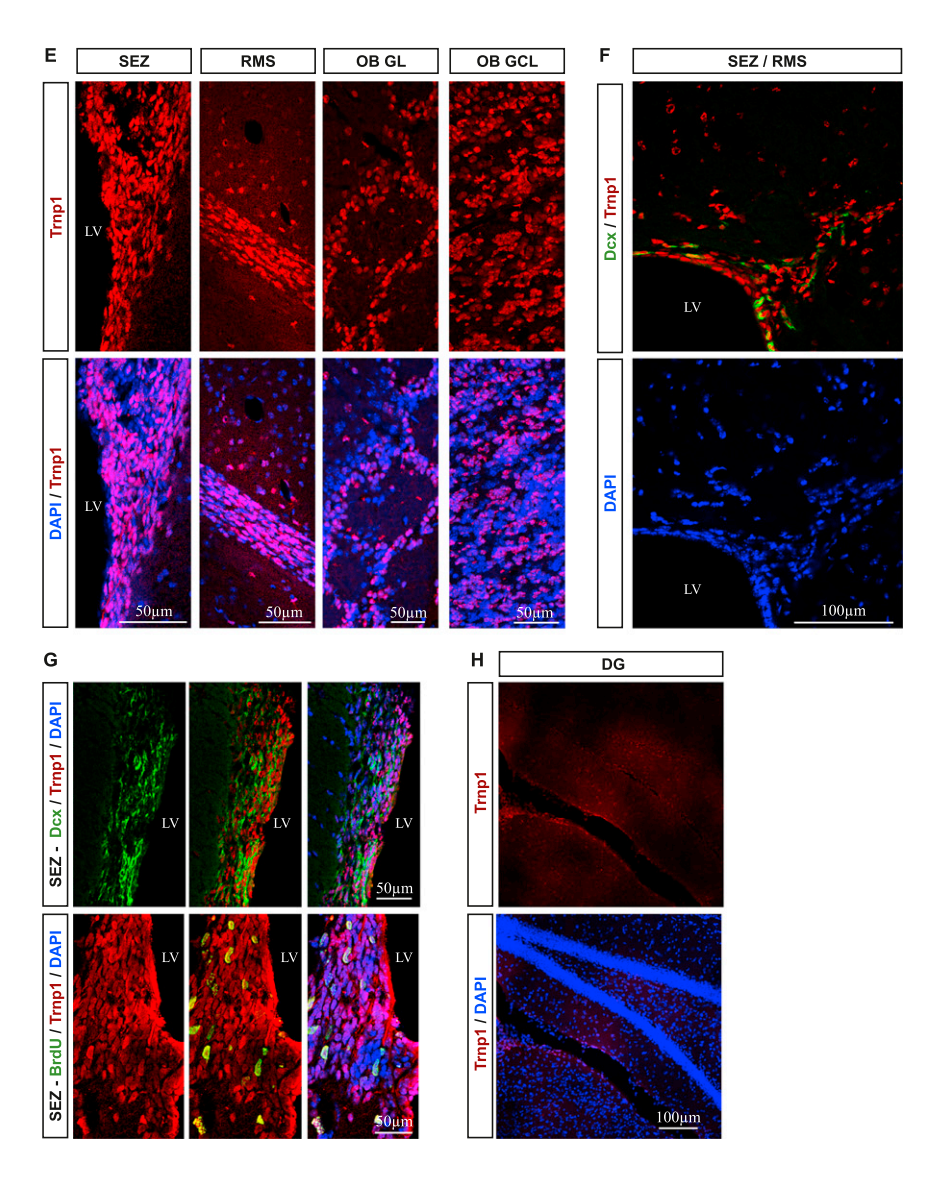


Figure S1. (continued).

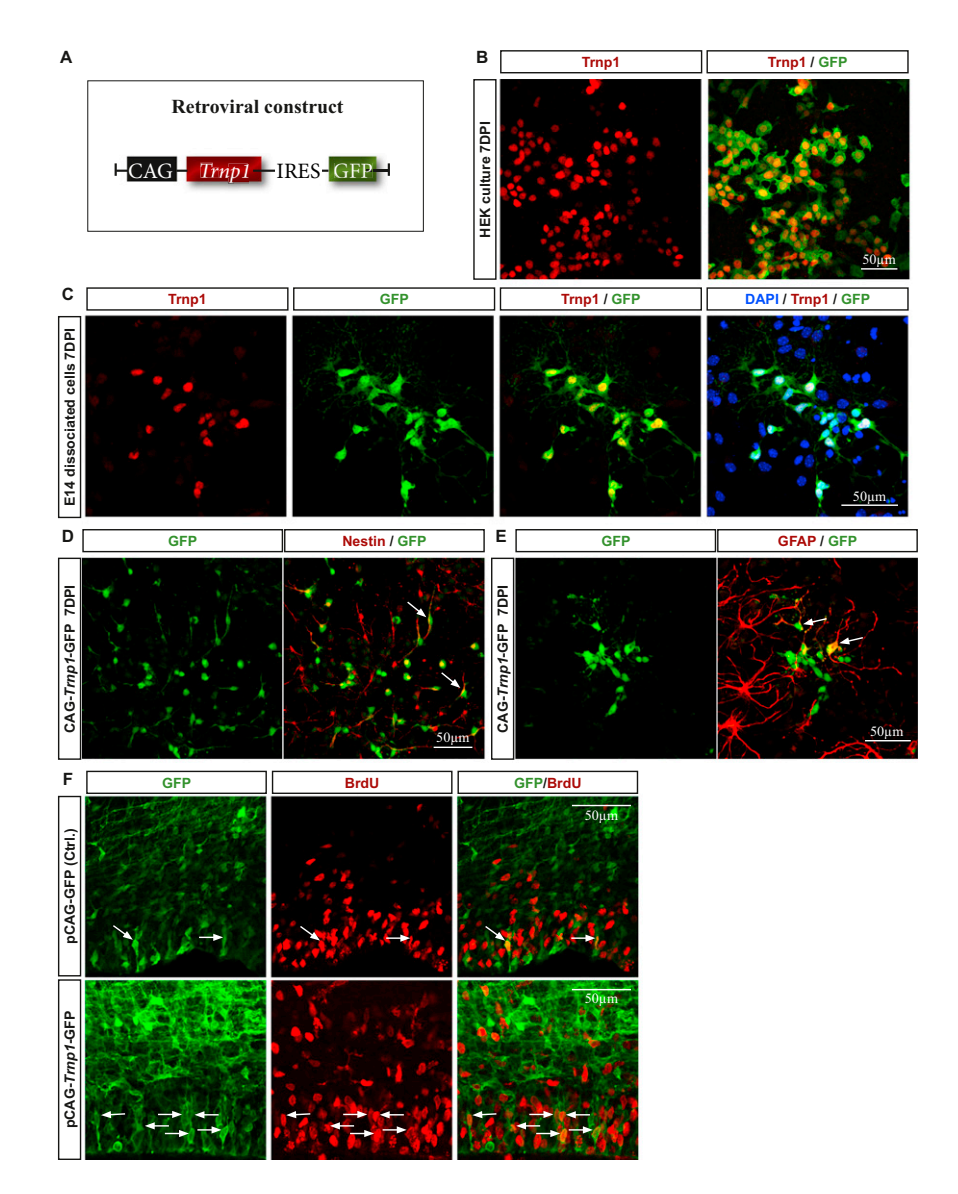


Figure S2. Generation of a Retroviral Vector for Forced Expression of Trnp1, Related to Figures 2 and 3

(A) Tmp1 cDNA lacking its 3'-UTR was cloned into a retroviral expression vector with the CAG promoter driving the transcription of Tmp1-IRES-GFP mRNA. GFP and Trnp1 are thus translated from the same mRNA produced from pCAG-Trnp1-GFP.

- (B) HEK cells were transduced with viral particles expressing Tmp1-IRES-GFP and immunostained for Trnp1 and GFP 7 days postinfection. Note that each GFP+ cell is also Trnp1+.
- (C) Dissociated cells from the cerebral cortex of E14 mouse embryos were infected with the same virus for overexpression of Trnp1. Reliable co-expression of Trnp1 and GFP in infected cells was tested by immunostaining 7 days postinfection.
- (D and E) Clones transduced with CAG-Tmp1-GFP were fixed 7 days posttransduction and colabeled for GFP and Nestin (D) or GFAP (E). Note that clones overexpressing Trnp1 still comprise some GFAP and Nestin positive cells 7 days posttransduction. CAG, chicken beta actin promoter; IRES, internal ribosomal entry site; DPI, days postinfection.
- (F) Micrographs depicting sections of the cerebral cortex 3 days after electroporation at E13 with either pCAG-IRES-GFP control or pCAG-Tmp1-IRES-GFP plasmid double labeled for GFP and BrdU. GFP and BrdU only as well as merge is shown and double positive cells quantified in Figure 3H are indicated by white arrows. The images shown correspond to Figures 3E and 3F to clarify the double positive character of the cells.

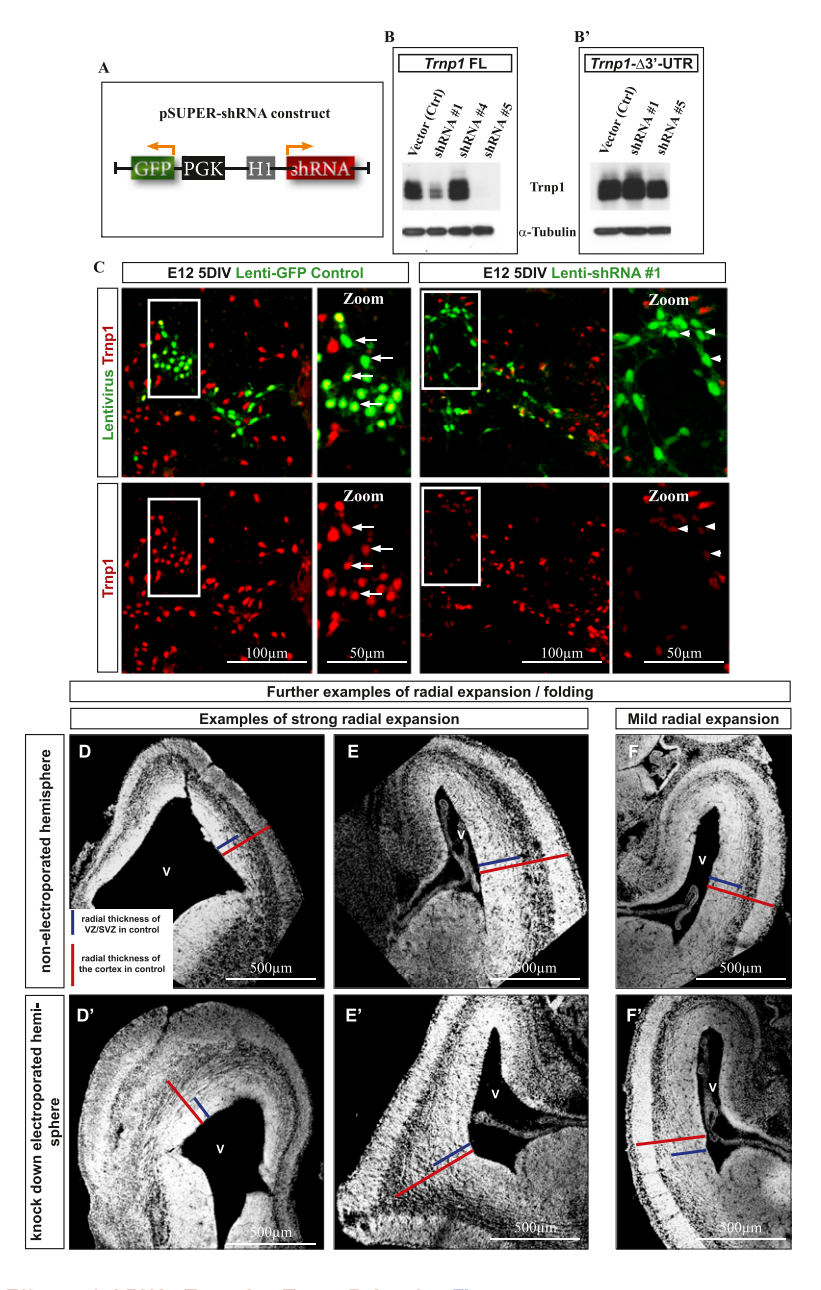


Figure S3. Specificity and Effects of shRNAs Targeting Trnp1, Related to Figure 4

(A) Three different shRNAs (each targeting the 3'-UTR of Trnp1) were cloned into pSUPER.GFP. The H1 promoter drives expression of the shRNA, GFP expression is driven by the PGK promoter from the same plasmid.

(B) Test of knock down efficiency of these shRNAs. HEK293 cells were cotransfected with pCMV-Trnp1 and pSUPER.GFP-shRNA plasmids or the empty pSUPER.GFP as a vector control. Note that shRNA#1 and #5 led to significant reduction in the Trnp1 band, whereas #4 was not effective in reducing Trnp1 levels. (B') Test of a version of Trnp1 lacking the shRNA-targeted 3'-UTR. HEK293 cells were cotransfected with pCAG-Tmp1-GFP (Tmp1Δ3'-UTR) and pSUPER.GFP shRNA plasmids or the empty pSUPER.GFP plasmid as a vector control. Note that neither shRNA#1 nor #5 were able to downregulate the resistant (Δ3'-UTR) Trnp1 version.

(C) ShRNAs were also sub-cloned into a lentiviral vector (pLVTHM) and viral particles were used to transduce dissociated cells from the embryonic cerebral cortex at embryonic day 12 in order to test for successful downregulation of endogenous Trnp1. As a control the same GFP-only expressing lentivirus was used. Five days posttransduction immunostaining for Trnp1 and GFP was performed revealing a clear reduction of endogenous Trnp1 detected by immunostaining in cells transduced with the shRNA#1. Arrows indicate GFP positive, Trnp1 positive cells, arrowheads indicate GFP positive cells with downregulated Trnp1 expression. (D-F') DAPI labeled coronal sections of embryonic brains electroporated with pSUPER.GFP-shRNA to downregulate Trnp1. (D)-(F) show the nonelectroporated hemispheres; (D'), (E'), and (F') show the electroporated hemispheres of the same (!) sections. Red bars indicate the radial length of the cortex and blue bars represent the size of the ventricular & subventricular zones (VZ/SVZ) of the nonelectroporated side. Bars of the length of the nonelectroporated hemispheres pasted into the electroporated hemispheres reveal the dramatic radial expansion in examples with a strong effect (D-E') and the milder expansion still comprising an increase in thickness of the SVZ as seen in few examples (see the blue bar in F' and compare it to the DAPI-dense progenitor zone).

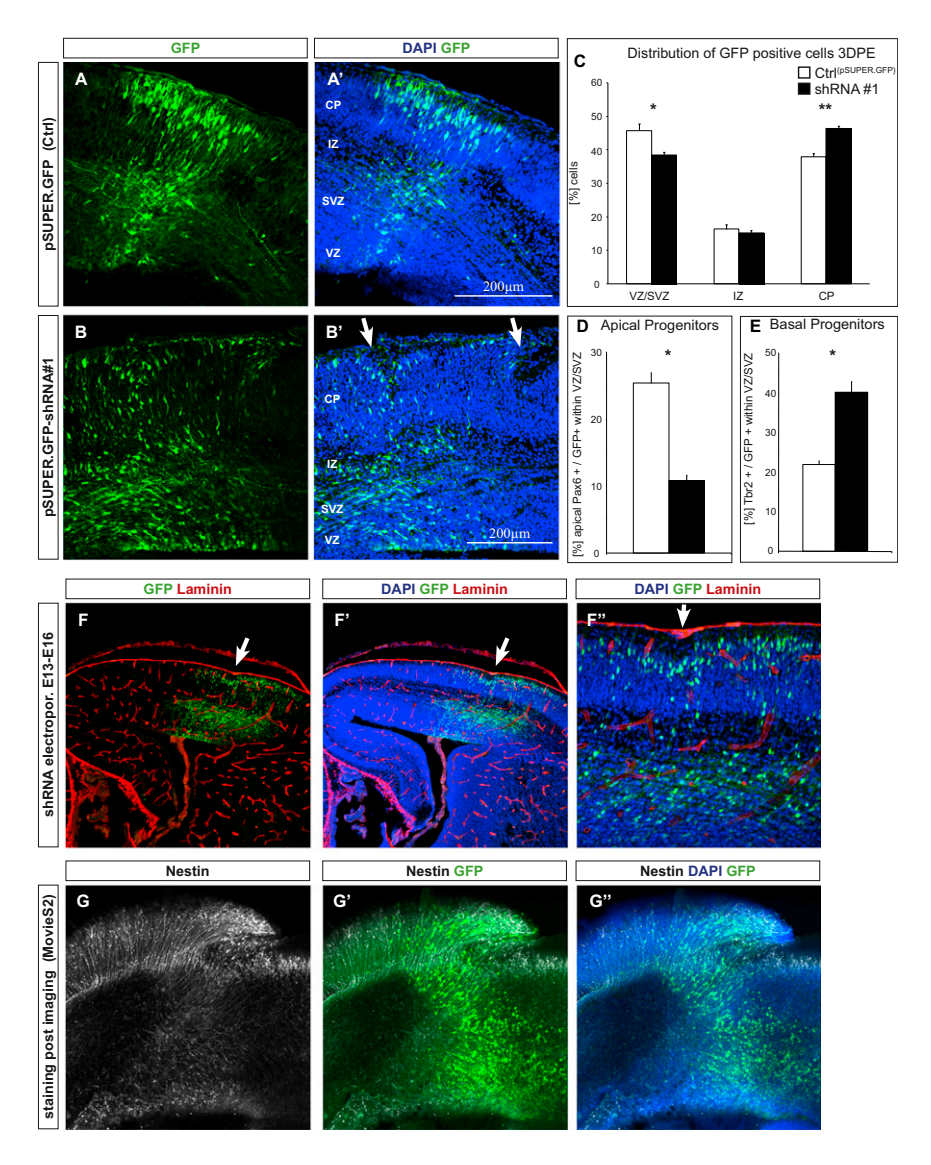


Figure S4. Representative Examples of shRNA-Electroporated Cerebral Cortices and Quantification of the Effects Obtained with Trnp1 shRNA #1, Related to Figure 5 and 4

(A-E) Coronal sections of embryonic cortices labeled with GFP and DAPI. Embryos were electroporated either with pSUPER.GFP control plasmid (A-A') or pSUPER.GFP-shRNA#1 (B-B') at E13 and analyzed at E16. Localization of cells was analyzed (C) and the number of apical progenitors (D) and basal progenitors (E) was characterized using Pax6 and Tbr2 immunolabeling respectively. Note, that use of shRNA#1 - a second, independent shRNA against Trnp1 - resulted in a similar effect with significantly more neurons in the cortical plate, less apical progenitors and more basal progenitors. Data are shown as mean ± SEM, n = 6 (shRNA#1) and 7 (control) embryos for cellular localization analysis (C) and n = 4 for apical- and basal progenitor analysis (D and E); *p < 0.05, **p < 0.01, Mann Whitney U-Test. White bars represent control (pSUPER.GFP) electroporated cells, black bars represent shRNA#1 electroporated cells.

(F-F") Micrographs depicting a coronal section of an embryonic brain electroporated with pSUPER.GFP-shRNA and labeled for DAPI, GFP and Laminin. Note the intact Laminin+ basement membrane overlying the electroporated region.

(G-G") Micrographs depicting the section imaged in Movie S1. Radial fibers are labeled by nestin (white in G). Note the fold that developed in the slice during imaging and the fanned array of nestin+ radial glial fibers reminiscent of their fanning-out array in gyri of naturally gyrated brains.

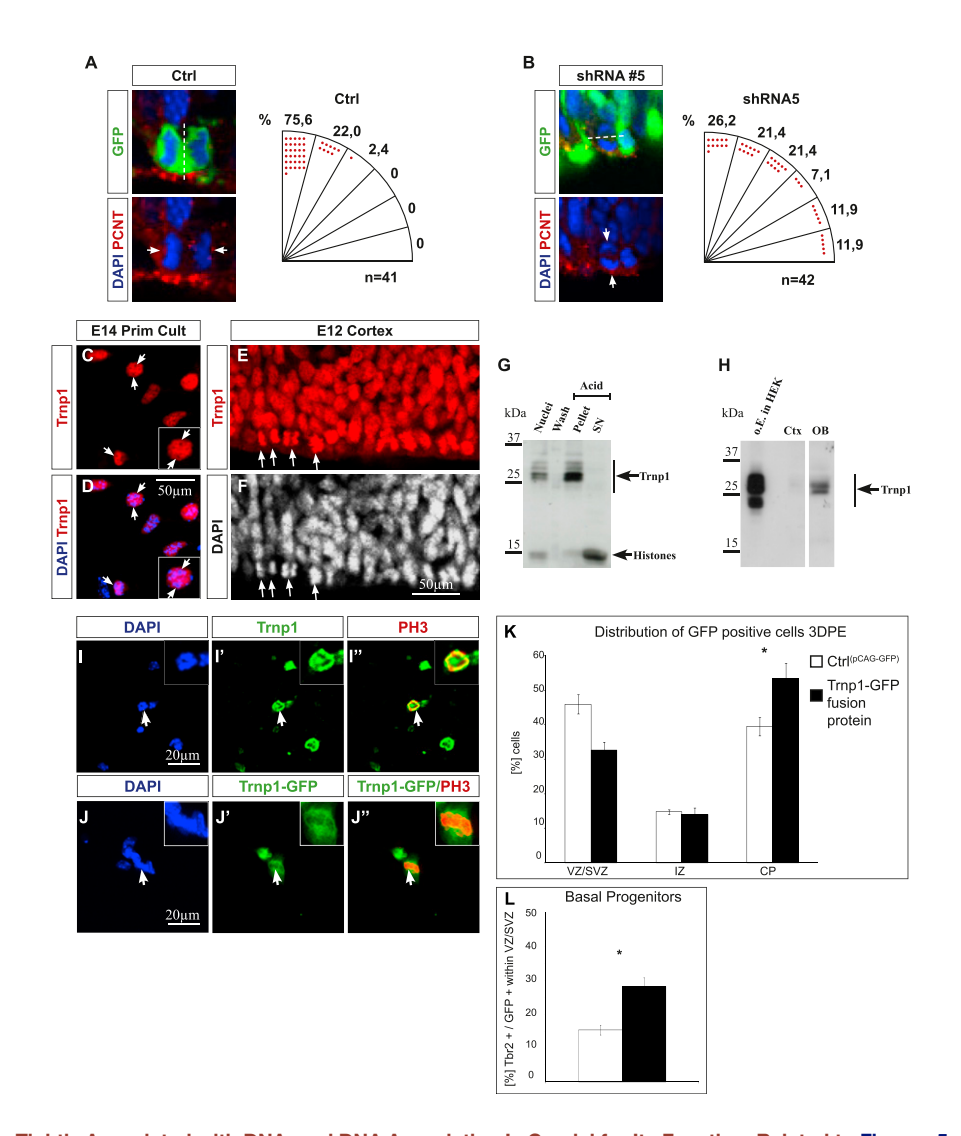


Figure S5. Trnp1 Is Tightly Associated with DNA, and DNA Association Is Crucial for Its Function, Related to Figures 5 and 6

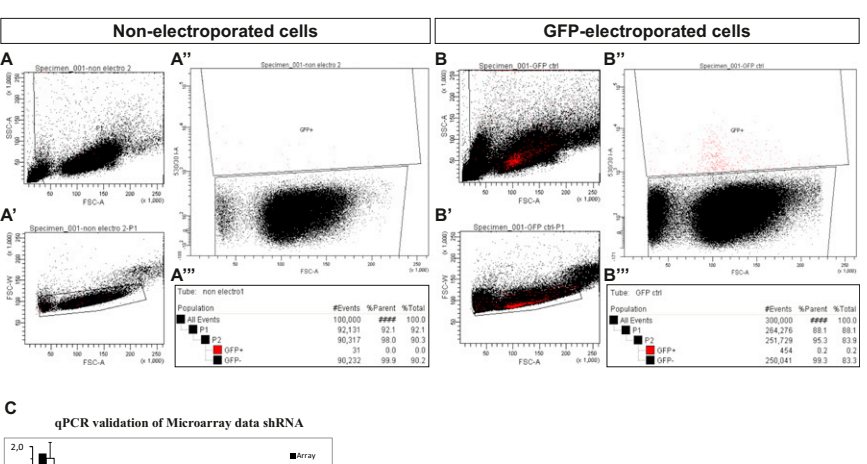
(A and B) Cleavage angle analysis of mitotic cells in brains of pSUPER.GFP shRNA#5 (B) and pSUPER.GFP control (A) electroporated embryos. Embryos were electroporated at E13 and analyzed at E14. Cleavage angle was analyzed utilizing DAPI (blue) to identify mitotic cells in ana- and telophase, GFP (green) to detect cells transfected with the GFP-expressing control or shRNA plasmids and Pericentrin (in red) to label the centrosomes. Note the increase in nonvertical cleavage planes of cells electroporated with shRNA targeting Trnp1.

(C and D) Dissociated cells from the E14 cerebral cortex transduced with CAG-Trnp1 retrovirus. Immunostaining for Trnp1 shows overexpressed Trnp1 localized in the nucleus but excluded in highly dense chromatin areas, which were localized by a strong DAPI signal (arrows). One cell is shown in a higher magnification. (E and F) Coronal sections of the cerebral cortex from E12 mouse embryos labeled for Trnp1 and DAPI. Note the clear association of Trnp1 with condensed chromatin as seen in anaphase chromosomes indicated by arrows. Single optical confocal sections are shown.

(G and H) Tissue from the E14 cerebral cortex (G) or from the adult cerebral cortex and adult OB (H) was lysed using different lysis buffers and protocols. Protein Ivsates were subjected to SDS-PAGE and analyzed by western blotting using anti-Trnp1 antibody. (G) Nuclei from E14 cortices were isolated using HRSB buffer and further processed utilizing an acidic protein extraction. Nuclei, wash and pellet and supernatant of the acidic extraction were subjected to western blot analysis using anti-Trnp1 antibody. Note that Trnp1 is mainly detectable in the insoluble fraction upon acidic treatment and that histones are detectable in the acidic soluble fraction (SN). SN: supernatant. (H) Adult cerebral cortical tissue (Ctx) and adult OBs were lysed using RIPA buffer containing 0.5M NaCl. Note that Trnp1 is present in OB lysates but absent in adult cerebral cortex lysates, consistent with the immunostaining shown in Figure 1I. As a positive control, lysates from HEK cells overexpressing Trnp1 were used (o.E. in HEK). One empty lane in between Ctx and OB lysate lanes was cropped for reasons of better comparison. The cropped lane is indicated by a space.

(I-J") Dissociated cells from the E14 cerebral cortex stained for endogenous Trnp1 and phospho-Histone 3 (PH3) (I-I") or transfected with a construct to express the Trnp1-GFP fusion protein stained for GFP and PH3 (J-J"). Cells were fixed 3 days posttransfection, stained and colabeled with DAPI. Arrows indicate an example of a cell during mitosis and inserts show a higher magnification of the same cell. Single optical sections are shown. Note the clear dissociation of Trnp1-GFP fusion protein from condensed chromatin during M-Phase.

(K and L) Embryos were electroporated with pCAG-Trnp1-GFP (fusion construct) or control pCAG-GFP plasmid at E13 and analyzed at E16. Localization of cells was analyzed (K) and the number of basal progenitors (L) was characterized using Tbr2 immunolabeling respectively. Note, that the Trnp1-GFP fusion protein was not able to reproduce the overexpression phenotype observed with Trnp1 (see Figure 3). Error bars represent SEM.



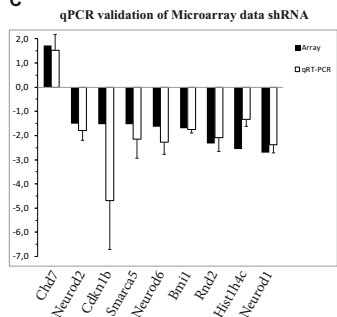


Figure S6. FACS of Cells for Transcriptome Analysis upon Trnp1 Knockdown, Related to Figure 6

(A-B") FACS sorting of GFP positive cells (B-B") from cortices electroporated at E13 and dissected one day later at E14. As a control and to set the gates, dissociated cells from nonelectroporated cortices were used (A-A"). (A and B) Live cells of the correct size and granularity were selected by setting forward (FSC-A) and sideward scatter (SSC-A). (A' and B') Cellular aggregates were excluded based on FSC-A and FSC-W. (A" and B") Gates for GFP sorting. (A"' and B"') Analysis of cell numbers and percentage of the sorted, GFP positive cells in the different gates. Red dots indicate GFP positive cells. (C) qPCR analysis of selected genes confirmed the validity of the microarray data shown in Figure 6. Error bars represent SEM.

5	Short-term	analysis (E13	3->E16)	Long-term analysis (E13->P0/P2/P5)			
Construct	Embryo	Radial Expansion	Folding visible	Construct	Embryo	Radial Expansion	Folding v
pSUPER- shRNA#5 (E13-E16)	1	yes	yes	pSUPER- shRNA#5 (E13-P2)	1	yes	yes (macro
	2	yes	-		2	yes	yes (macro
	3	yes	yes		3	no	-
	4	no	-	pSUPER- shRNA#1 (E13-P0)	4	yes	yes (macro
	5	yes	-		5	yes	yes (macro
	6	yes	-		6	yes	yes
	7	yes	-		7	yes	-
	8	yes	yes	pSUPER- shRNA#1 (E13-P5)	8	yes	yes (macro
pSUPER-	9	yes	yes		9	yes	yes (macro
	10	yes	yes		10	no	-
	11	yes	yes			8 of 10	7 of 1
shRNA#1	12	yes	yes				
(E13-E16)	13	yes	yes	1			
	14	yes	-	1			
		13 of 14	8 of 14	1			
	1	no	-	1			
	2	no	-	1			
	3	no	-				
	4	no	-	1			
pSUPER- GFP Control (E13-E16)	5	no	-	1			
	6	no	-	1			
	7	no	-	1			
	8	no	-	1			
	9	no	-	1			
	10	no	-				
	11	no	-				
	12	no	-				
	13	no	-	1			
				•			

14

15

no

no 0 of 15

Table S1. Overview of Phenotypes Observed after Electroporation of shRNAs Targeting Trnp1 or Control Electroporations, Related to Figures 4 and 5

0 of 15

Folding visible

yes (macroscopic) yes (macroscopic)

yes (macroscopic)

yes (macroscopic)

yes (macroscopic)

yes (macroscopic)

7 of 10

Short-term (left columns) or long-term analysis of knockdown (shRNA#1 and shRNA#5) and control electroporated brains. Phenotypes were scored for radial expansion as demonstrated in Figures 4 and S3 and folding as demonstrated in Figures 5 and S4. In total, we observed a radial expansion of the cortex in 21 and folding in 15 out of 24 shRNA electroporated brains compared to 0 out of 15 control electroporated brains. Strikingly, folds were even visible by eye when brains were dissected postnatally and are indicated as macroscopic folds observed in 6 of 10 brains analyzed at postnatal stages.

Gene	Expression KD Trnp1 vs		
2610044O15Rik	Ctrl 0,30		
ccdc101			
Tceal1	0,43		
	0,44		
Gtf2b	0,49		
Sec23ip	0,51		
Sf3b4	0,53		
Phyh 4933403F05Rik	0,54		
Zfp87	0,55 0,55		
Asb3			
Hist4h4	0,55		
	0,56		
Zfp422	0,57		
Tmem129	0,58		
Golph31	0,59		
Gstp2	0,59		
Hist1h1b	0,60		
Ndufa1	0,60		
drg2	0,62		
Pgs1	0,62		
Cenk	0,62		
Rangap1	0,62		
Dusp14	0,36		
Neurod1	0,37		
Nrp1	0,38		
Ypel4	0,42		
Ap3s1	0,44		
Rasgef1b	0,50		
Plekhf2	0,53		
Unc5d	0,53		
Cdkn2d	0,57		
Ptcd2	0,57		
Trp53inp1	0,58		
Nhlh1	0,58		
Pcp4	0,58		
St6gal1	0,60		
Neurod6	0,61		
Tagln3	0,61		
plxna4	0,62		
Zfp238	0,63		
Nuak1	0,31		
Chrnb2	0,43		
Rnd2	0,43		
Vash2	0,43		
Chst15	0,45		
Robo2	0,46		
Chga	0,48		
Josd1	0,49		

Gene	Expression KD Trnp1 vs Ctrl			
Trio	0,51			
Map2k6	0,56			
	0,59			
Atf2	0,60			
6330403K07Rik	0,62			
Commd6	0,32			
Hist1h4c	0,39			
Mis12	0,44			
Fam110a	0,51			
Hist1h4f	0,52			
Mpv1712	0,54			
Zfp518b	0,55			
Fbxo46	0,56			
Ecsit	0,56			
Psmg3	0,57			
Zfp71-rsl	0,58			
Mtvr2	0,58			
Rab8a	0,58			
Glod4	0,59			
Bmi1	0,59			
ccdc32	0,59			
Vat1	0,59			
Ttc28	0,59			
ENSMUST00000121	0,60			
Plekha8	0,60			
Zmat3	0,60			
Nkrf	0,61			
2810006K23Rik	0,61			
Sec22c	0,61			
Sap30	0,62			
cdc37	0,62			
Brms1	0,62			
ENSMUST00000116	0,62			
Fam108a	0,62			
ENSMUST00000121	0,62			
Fam84a	0,62			

Highest Expressed in	Ventricular zone	
Highest Expressed in	SVZ	
Highest Expressed in	Neurons	
Bold	Transcriptional regulation	
Italic	Signaling	

Stahl et al Table S2

Table S2. Overview of Highly Significant Downregulated Genes, Related to Figure 6

List of genes significantly downregulated upon Trnp1 knockdown, with colors indicating the layer/cell type of highest expression. (Blue) Highest expressed in ventricular zone; (red) highest expressed in subventricular zone; (yellow) highest expressed in neurons within the cortical plate. Bold represents genes with products involved in transcriptional regulation, and italics represent those involved in signaling.